

# SUPPLEMENTARY MATERIAL:

## Metrological characterization of non-Gaussian entangled states of superconducting qubits

Kai Xu,<sup>1,\*</sup> Yu-Ran Zhang,<sup>2,\*</sup> Zheng-Hang Sun,<sup>1,\*</sup> Hekang Li,<sup>1</sup> Pengtao Song,<sup>1</sup> Zhongcheng Xiang,<sup>1</sup> Kaixuan Huang,<sup>1</sup> Hao Li,<sup>1</sup> Yun-Hao Shi,<sup>1</sup> Chi-Tong Chen,<sup>1</sup> Xiaohui Song,<sup>1</sup> Dongning Zheng,<sup>1</sup> Franco Nori,<sup>2,3,†</sup> H. Wang,<sup>4,‡</sup> and Heng Fan<sup>1,5,§</sup>

<sup>1</sup>*Institute of Physics, Chinese Academy of Sciences, Beijing 100190, China*

<sup>2</sup>*Theoretical Quantum Physics Laboratory, RIKEN Cluster for Pioneering Research, Wako-shi, Saitama 351-0198, Japan*

<sup>3</sup>*Physics Department, University of Michigan, Ann Arbor, Michigan 48109-1040, USA*

<sup>4</sup>*Interdisciplinary Center for Quantum Information, State Key Laboratory of Modern Optical Instrumentation, and Zhejiang Province Key Laboratory of Quantum Technology and Device, Department of Physics, Zhejiang University, Hangzhou 310027, China*

<sup>5</sup>*Beijing Academy of Quantum Information Sciences, and CAS Center for Excellence in Topological Quantum Computation, University of Chinese Academy of Sciences, Beijing 100190, China*

(Dated: January 19, 2022)

### CONTENTS

I. Comparison of metrological gains over the quantum standard limit with other experiments	1
II. Experimental device	3
III. Phase calibration	4
IV. Measurement of linear and nonlinear spin squeezing parameters	5
A. Optimization of metrological squeezing parameters	5
B. Linear Ramsey squeezing parameter	6
C. Second-order nonlinear squeezing parameter	7
D. Efficient detection of second-order nonlinear squeezing parameter with seven operators	12
E. Experimental details on measurement of squeezing parameters	12
F. Observables for the optimal metrological squeezing parameters	13
V. Extraction of the Fisher information	15
A. Extraction of the Fisher information from the squared Hellinger distance	15
B. Experimental details for extracting the Fisher information	18
References	18

### I. COMPARISON OF METROLOGICAL GAINS OVER THE QUANTUM STANDARD LIMIT WITH OTHER EXPERIMENTS

Our experiments generate multiparticle entangled states of up to 19 superconducting qubits through the short-time nonlinear evolution of the system with the Hamiltonian in Eq. (1) of the main text. To characterize the useful entangled states for quantum metrology with superconducting qubits, we measure the linear and nonlinear spin squeezing parameters (discussed in Section IV) and extract the Fisher information from the squared Hellinger distance (discussed in Section V), which all indicate the metrological gain over the quantum standard limit (SQL) of the phase sensitivity  $\Delta\theta_{\text{SQL}} \sim 1/\sqrt{N}$ , with  $N$  being the number of particles.

In our experiments, the Fisher information of non-Gaussian entangled states in the over-squeezed regime reveals the largest metrological gains. In Fig. S1, our experimental results,  $F/N = 7.10^{+0.26}_{-0.28}$  dB with  $N = 10$  qubits, and  $F/N = 9.89^{+0.28}_{-0.29}$  dB with  $N = 19$  qubits, are compared with other experimental results [1–35], obtained on different experimental platforms including cold/thermal atoms, trapped ions, Bose-Einstein condensates, photonic systems, Rydberg atoms, and superconducting

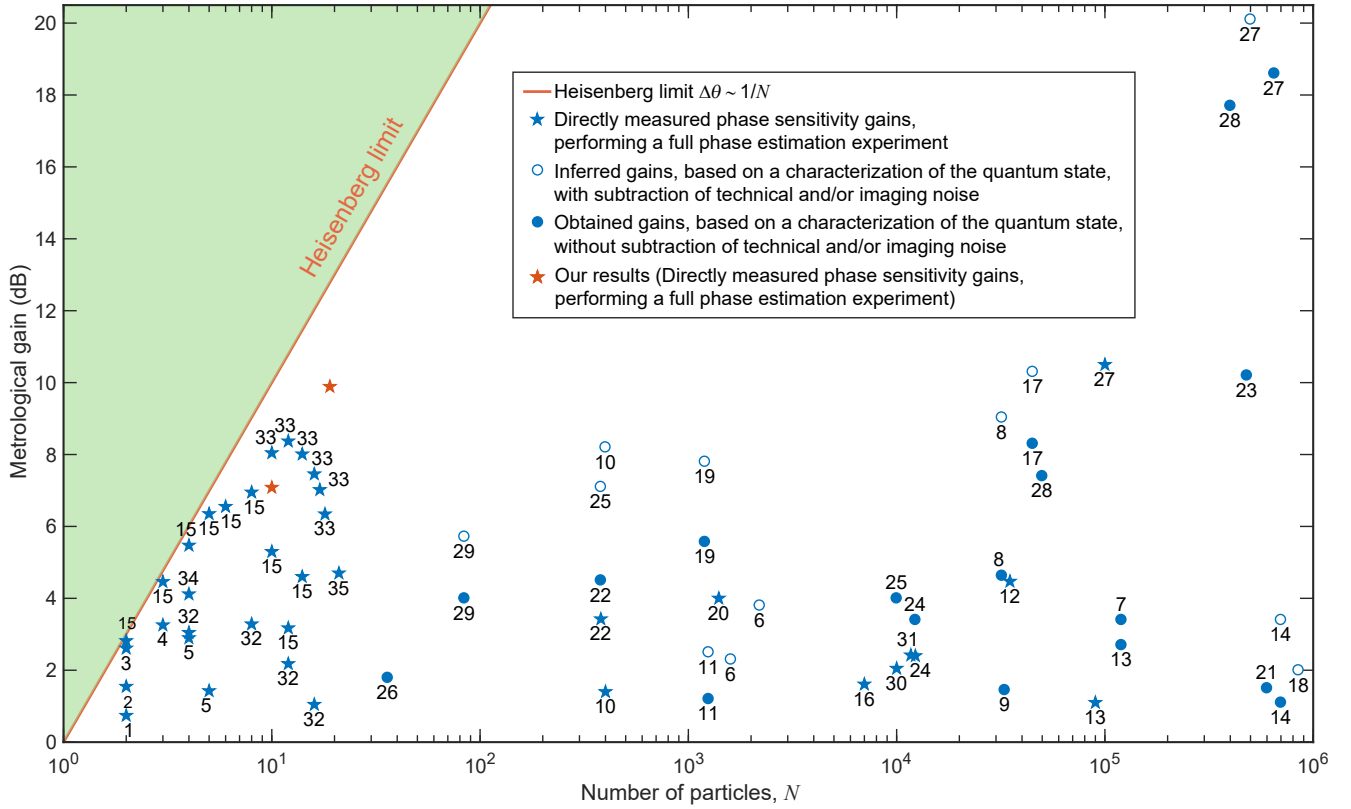
---

\* These authors contributed equally to this work.

† fnori@riken.jp

‡ hhwang@zju.edu.cn

§ hfan@iphy.ac.cn



- [1] Sackett *et al.*, Nature **404**, 256 (2000).  
[2] Meyer *et al.*, Phys. Rev. Lett. **86**, 5870 (2001).  
[3] Leibfried *et al.*, Nature **422**, 412 (2003).  
[4] Leibfried *et al.*, Science **304**, 1476 (2004).  
[5] Leibfried *et al.*, Nature **438**, 639 (2005).  
[6] Estève *et al.*, Nature **455**, 1216 (2008).  
[7] Appel *et al.*, PNAS **106**, 10960 (2009).  
[8] Leroux *et al.*, Phys. Rev. Lett. **104**, 073602 (2010).  
[9] Schleier-Smith *et al.*, Phys. Rev. Lett. **104**, 073604 (2010).  
[10] Gross *et al.*, Nature **464**, 1165 (2010).  
[11] Riedel *et al.*, Nature **464**, 1170 (2010).  
[12] Leroux *et al.*, Phys. Rev. Lett. **104**, 250801 (2010).  
[13] Louchet-Chauvet *et al.*, New J. Phys. **12**, 065032 (2009).  
[14] Chen *et al.*, Phys. Rev. Lett. **106**, 133601 (2011).  
[15] Monz *et al.*, Phys. Rev. Lett. **106**, 130506 (2011).  
[16] Lücke *et al.*, Science **334**, 773 (2011).  
[17] Hamley *et al.*, Nat. Phys. **8**, 305 (2012).  
[18] Sewell *et al.*, Phys. Rev. Lett. **109**, 253605 (2012).  
[19] Berrada *et al.*, Nat. Commun. **4**, 2077 (2013).  
[20] Ockeloen *et al.*, Phys. Rev. Lett. **111**, 143001 (2013).  
[21] Sewell *et al.*, Phys. Rev. X **4**, 021045 (2014).  
[22] Strobel *et al.*, Science **345**, 424 (2014).  
[23] Bohnet *et al.*, Nat. Photon. **8**, 731 (2014).  
[24] Muessel *et al.*, Phys. Rev. Lett. **113**, 103004 (2014).  
[25] Muessel *et al.*, Phys. Rev. A **92**, 023603 (2015).  
[26] Barontini *et al.*, Science **349**, 1317 (2015).  
[27] Hosten *et al.*, Nature **529**, 505 (2016).  
[28] Cox *et al.*, Phys. Rev. Lett. **116**, 093602 (2016).  
[29] Bohnet *et al.*, Science **352**, 1297 (2016).  
[30] Kruse *et al.*, Phys. Rev. Lett. **117**, 143004 (2016).  
[31] Zou *et al.*, PNAS **115**, 6381 (2018).  
[32] Omran *et al.*, Science **365**, 570 (2019).  
[33] Song *et al.*, Science **365**, 574 (2019).  
[34] Krischek *et al.*, Phys. Rev. Lett. **107**, 080504 (2011).  
[35] Liu *et al.*, Nat. Photon. **15**, 137 (2021).

FIG. S1. Metrological gains of the phase sensitivity over the standard quantum limit. Comparing the metrological gains of phase sensitivity  $\Delta\theta$  over the standard quantum limit  $\Delta\theta_{SQL} \sim 1/\sqrt{N}$  with other experiments, which are shown on logarithmic scales,  $10 \log_{10}(\Delta\theta_{SQL}/\Delta\theta)^2$  dB. The solid red line shows the Heisenberg limit  $\Delta\theta_{HL} \sim 1/N$ . Each symbol is accompanied by a number, corresponding to the reference list below, where Refs. [1–31] are in the same order and displayed using the same data and symbols as in Ref. [36].

qubits. Here, the experimental results in Refs. [1–31] have been reviewed in Fig. 2 of Ref. [36] (with the same list number). In addition, our comparison also includes several recent experimental results in Refs. [32–35].

Our work shows that superconducting qubits, with high-fidelity controls and long decoherence times, are able to efficiently perform quantum metrology tasks, since our *metrological gain with 19 superconducting qubits is larger than the ones obtained on other platforms with up to 10,000 particles*. In addition, the ability to perform *single-shot readout measurement on each qubit* on the superconducting processor also makes the detection of *nonlinear squeezing parameters and other quantum-information tasks* possible. These advantages indicate the potential of an all-to-all connected superconducting circuit architecture for exploring

quantum many-body physics, and also for practical applications in quantum metrology and quantum information processing.

## II. EXPERIMENTAL DEVICE

The device contains 20 superconducting qubits ( $q_j$  with  $j$  varied from 1 to 20), which are fully connected through a common resonator bus R. In our experiments, we use 19 of them, as one qubit ( $q_7$ ) suffers from a strong interaction with a two-level system near its working point. The qubit characteristics can be found in Ref. [33], which is the same device used in this experiment. Table S1 lists the latest device information for the participating qubits, obtained during this experiment. The full Hamiltonian of our quantum processor can be written as

$$\begin{aligned} \hat{H}_0 = & \omega_r \hat{a}^\dagger \hat{a} + \sum_{j=1}^{19} \omega_j \hat{\sigma}_j^+ \hat{\sigma}_j^- + \sum_{j=1}^{19} g_j (\hat{\sigma}_j^+ \hat{a} + \hat{\sigma}_j^- \hat{a}^\dagger) \\ & + \sum_{i < j} \chi_{ij}^c (\hat{\sigma}_i^+ \hat{\sigma}_j^- + \hat{\sigma}_j^+ \hat{\sigma}_i^-), \end{aligned} \quad (\text{S1})$$

where  $\omega_j/2\pi$  denotes the resonant frequency of  $q_j$  (individually tunable from 3 GHz to 5.5 GHz). The frequency of the common resonator bus R, represented by  $\omega_r/2\pi$ , is fixed at about 5.51 GHz. Each qubit  $q_j$  is capacitively coupled to R, with magnitude,  $g_j/2\pi$ , listed in Table S1. Note that except for the dominant qubit-resonator interaction, there exist small direct couplings,  $\chi_{ij}^c/2\pi$ , between qubits in the system. In our experiments, by equally detuning the frequencies of all qubits far away from that of the resonator, we can realize the resonator-induced super-exchange interaction with a magnitude of  $g_i g_j/(2\pi\Delta)$  (with  $\Delta = \omega_i - \omega_r = \omega_j - \omega_r$ , and  $|\Delta| \gg g_i, g_j$ ) between *any* two qubits. The Hamiltonian can be further written as

$$\hat{H} = \sum_{i < j} (g_i g_j / \Delta + \chi_{ij}^c) (\hat{\sigma}_i^+ \hat{\sigma}_j^- + \hat{\sigma}_j^+ \hat{\sigma}_i^-). \quad (\text{S2})$$

The qubit-qubit coupling strengths

$$\chi_{ij} \equiv g_i g_j / \Delta + \chi_{ij}^c, \quad (\text{S3})$$

	$\omega_j/2\pi$ (GHz)	$T_{1,j}$ (μs)	$g_j/2\pi$ (MHz)	$\omega_j^r/2\pi$ (GHz)	$\omega_j^m/2\pi$ (GHz)	$F_{0,j}$	$F_{1,j}$
q <sub>1</sub>	4.350	≈ 20	27.6	6.768	4.460	0.977	0.921
q <sub>2</sub>	4.390	≈ 26	27.4	6.741	4.310	0.986	0.879
q <sub>3</sub>	4.275	≈ 27	29.1	6.707	4.355	0.975	0.912
q <sub>4</sub>	4.300	≈ 26	27.6	6.676	4.440	0.989	0.918
q <sub>5</sub>	4.245	≈ 26	26.5	6.649	4.260	0.975	0.909
q <sub>6</sub>	5.081	≈ 27	29.2	6.612	4.805	0.975	0.925
q <sub>8</sub>	4.215	≈ 26	30.1	6.558	4.285	0.987	0.906
q <sub>9</sub>	5.120	≈ 23	24.1	6.552	5.070	0.989	0.926
q <sub>10</sub>	5.160	≈ 30	27.7	6.514	5.290	0.995	0.903
q <sub>11</sub>	5.290	≈ 24	27.3	6.525	5.170	0.994	0.897
q <sub>12</sub>	5.215	≈ 35	26.9	6.550	5.210	0.981	0.920
q <sub>13</sub>	4.945	≈ 26	29.1	6.568	4.895	0.980	0.916
q <sub>14</sub>	5.250	≈ 41	27.4	6.598	5.250	0.983	0.896
q <sub>15</sub>	4.895	≈ 31	26.3	6.641	4.235	0.978	0.913
q <sub>16</sub>	4.325	≈ 25	26.5	6.660	4.850	0.987	0.934
q <sub>17</sub>	4.735	≈ 36	27.3	6.686	4.578	0.984	0.942
q <sub>18</sub>	4.815	≈ 38	29.0	6.713	4.770	0.982	0.912
q <sub>19</sub>	4.425	≈ 35	24.6	6.788	4.385	0.98	0.900
q <sub>20</sub>	4.855	≈ 30	27.5	6.759	5.115	0.985	0.918

TABLE S1. Qubit characteristics.  $\omega_j/2\pi$  is the idle frequency of  $q_j$ , where single-qubit rotation pulses are applied.  $T_{1,j}$  is the energy relaxation time of  $q_j$ , which is the typical value across a wide frequency range.  $g_j/2\pi$  denotes the coupling strength between  $q_j$  and the resonator bus R.  $\omega_j^r/2\pi$  is the resonant frequency of  $q_j$ 's readout resonator.  $\omega_j^m/2\pi$  is the resonant frequency of  $q_j$  at the beginning of the measurement process, when its readout resonator is pumped with microwave pulse.  $F_{0,j}$  ( $F_{1,j}$ ) is the probability of detecting  $q_j$  in  $|0\rangle$  ( $|1\rangle$ ) state, when it is prepared in the  $|0\rangle$  ( $|1\rangle$ ) state.

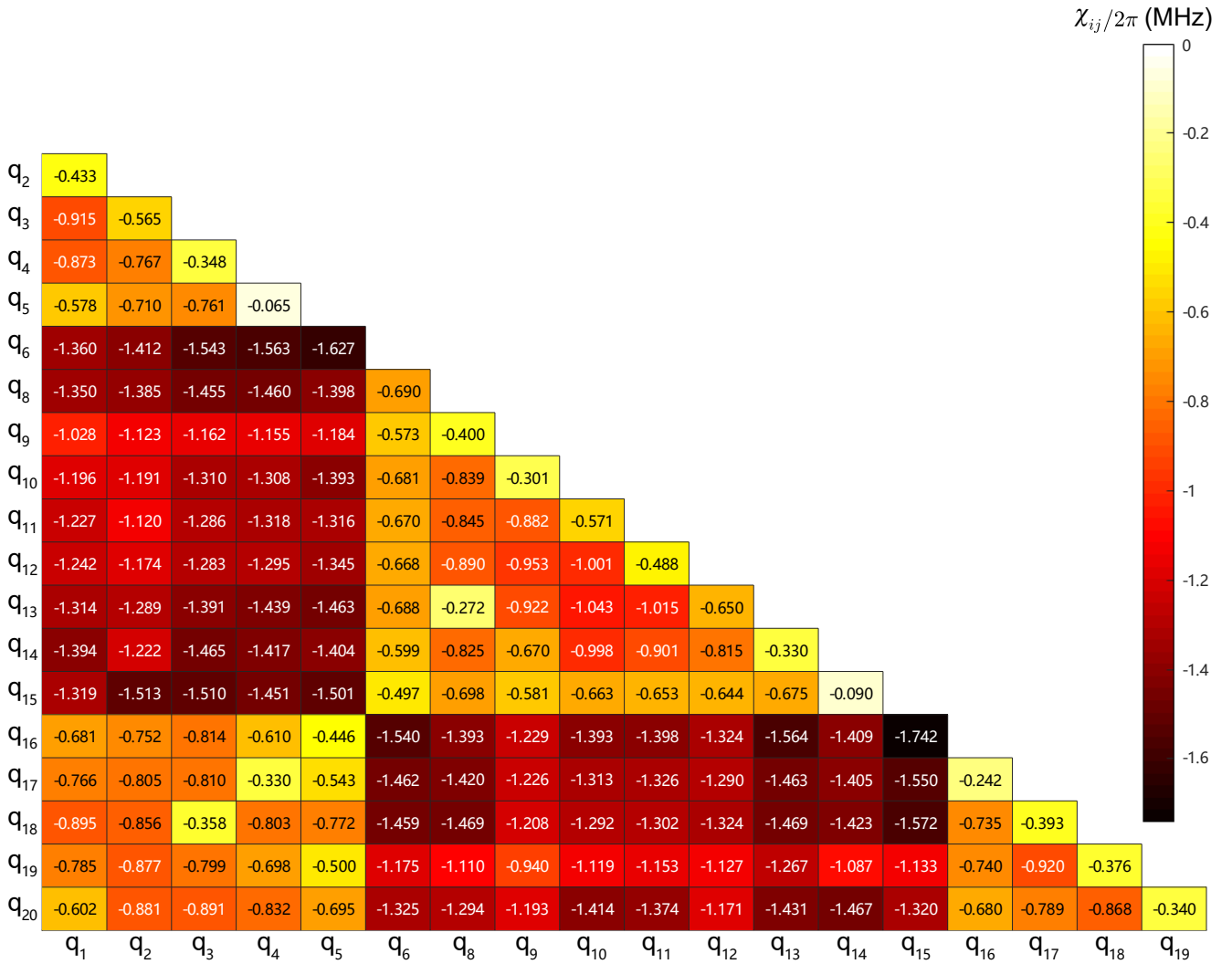


FIG. S2. Coupling matrix. Plotted is the coupling strength  $\chi_{ij}/2\pi$  between  $q_i$  and  $q_j$  in the quantum processor, which is measured by the energy swapping process, where  $q_i$  and  $q_j$  are equally tuned at the working point  $\omega_I$  to interact for a specific time [37].

which can be experimentally estimated by the energy swapping process between  $q_i$  and  $q_j$  (see Supplementary materials of Ref. [37]), are shown in Fig. S2, with  $\Delta/2\pi \simeq -580$  MHz in this experiment.

For the 10-qubit experiment, we choose  $q_6, q_9, q_{10}, q_{11}, q_{12}, q_{13}, q_{14}, q_{17}, q_{18}$ , and  $q_{20}$ . For the 19-qubit experiment, we choose 19 qubits except for  $q_7$ . In the main text, for convenience, the 19 qubits in order  $\{q_6, q_9, q_{10}, q_{11}, q_{12}, q_{13}, q_{14}, q_{17}, q_{18}, q_{20}, q_1, q_2, q_3, q_4, q_5, q_8, q_{15}, q_{16}, q_{19}\}$  are relabeled as  $\{Q_j\}$  with  $j = 1, 2, \dots, 19$ .

### III. PHASE CALIBRATION

In our experiments, the nonlinear evolution  $\exp(-i\hat{H}t)$  is realized by equally detuning all the qubits from their idle points,  $\omega_j/2\pi$ , to the interacting point,  $\omega_I/2\pi$ , by applying a rectangular pulse to each qubit. This operation will accumulate some dynamical phase, which needs to be cancelled via applying rotation pulses after the rectangular pulses. In theory, the dynamical phase can be estimated as  $2\pi\delta f \times t$ , where  $\delta f = (\omega_j - \omega_I)/2\pi$ . However, the imperfections of rectangular pulses, such as the imperfect rising and falling edges, will cause an additional phase shift from the theoretical calculations, which also needs to be experimentally calibrated. Figure S3 shows the pulse sequence and the results of our phase calibration method, taking  $q_1$  as an example.  $q_1$  is tuned to the interacting point, while other qubits are arranged at their frequency points  $\omega_j^o/2\pi$  far away from  $\omega_I/2\pi$ . To minimize the Z-crosstalk effects of other qubits to  $q_j$  when being tuned away,  $\omega_j^o/2\pi$  are selected to have an equal Z-crosstalk effect on  $q_1$ , compared to the case when all qubits are tuned to  $\omega_I/2\pi$ , as can be estimated by the measured

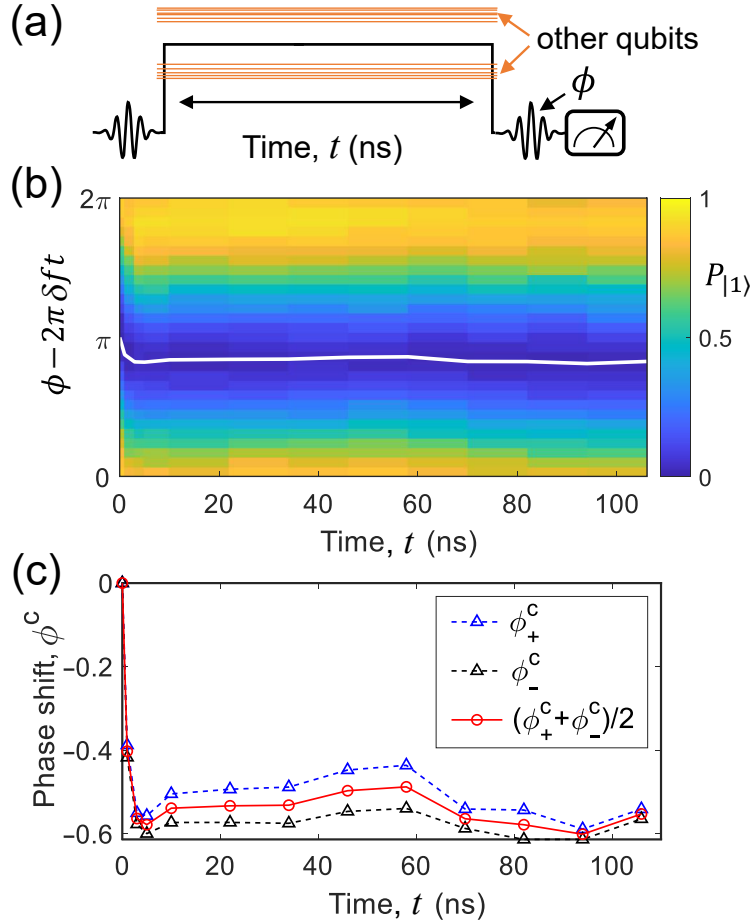


FIG. S3. Dynamical phase calibration. (a,b) Experimental results and sequence of phase calibration for q<sub>1</sub>. (c) The phase shift  $\phi^c$  obtained by fitting the results in (b) as a function of the interaction time  $t$ .

Z-crosstalk matrix  $M_Z$ . We monitor the  $|1\rangle$  state probability  $P(\phi, t)$  as a function of both the time  $t$  and the phase difference  $(\phi - 2\pi\delta f \times t)$ . For each time  $t$ , we perform a cosine fit to  $P(\phi, t)$  as a function of  $\phi$  to extract the phase shift  $\phi_+^c$ , caused by the imperfect rectangular pulses. To further reduce the Z-crosstalk effects and the ac-stark shift effects due to imperfect decoupling of other qubits to q<sub>1</sub> when being tuned away, we perform this calibration process again with a little difference. The frequencies of other qubits are arranged at  $(2\omega_I - \omega_j^0)/2\pi$ , a symmetric position relative to  $\omega_I/2\pi$ . Again, we obtain the phase shift  $\phi_-^c$ . The final phase shift, used to cancel the dynamical phase, is  $(\phi_+^c + \phi_-^c)/2$ , as shown by the red curves in Fig. S3(c).

#### IV. MEASUREMENT OF LINEAR AND NONLINEAR SPIN SQUEEZING PARAMETERS

##### A. Optimization of metrological squeezing parameters

To estimate the phase  $\theta$ , imprinted on a state with a density matrix  $\rho_\theta$ , by measuring an observable  $\hat{X}$ , the phase sensitivity (for the unbiased estimation) can be given by [36]

$$\Delta^2\theta = \frac{1}{\nu} \frac{(\Delta_{\rho_\theta} \hat{X})^2}{(\partial_\theta \langle \hat{X} \rangle_{\rho_\theta})^2} \equiv \frac{\xi^2[\rho_\theta, \hat{X}]}{\nu}, \quad (\text{S4})$$

where  $\nu$  is the number of trials of the measurement. Here, the coefficient

$$\xi^2[\rho_\theta, \hat{X}] \equiv \frac{(\Delta_{\rho_\theta} \hat{X})^2}{(\partial_\theta \langle \hat{X} \rangle_{\rho_\theta})^2} \quad (\text{S5})$$

is defined as the metrological squeezing parameter of  $\rho$  with respect to the observable  $\hat{X}$  [38]. We consider the case that the phase is generated by a unitary process  $\rho_\theta = e^{-i\hat{G}\theta} \rho e^{i\hat{G}\theta}$  by a generator  $\hat{G}$ , and the squeezing parameter, in the limit  $\theta \rightarrow 0$ , can be obtained as

$$\xi^2[\rho, \hat{X}, \hat{G}] = \frac{(\Delta_\rho \hat{X})^2}{|\langle [\hat{X}, \hat{G}] \rangle_\rho|^2}, \quad (\text{S6})$$

where we have used the fact that  $(\Delta_{\rho_\theta} \hat{X})^2 \rightarrow (\Delta_\rho \hat{X})^2$ , and  $\partial_\theta \langle \hat{X} \rangle_{\rho_\theta} \rightarrow -i \langle [\hat{X}, \hat{G}] \rangle_\rho$ .

We then introduce a family of  $D$  accessible operators

$$\hat{\mathbf{S}} = (\hat{S}_1, \hat{S}_2, \hat{S}_3, \dots, \hat{S}_D), \quad (\text{S7})$$

with which the observable can be expressed as

$$\hat{X} = \hat{S}_{\hat{m}} = \hat{m} \cdot \hat{\mathbf{S}}, \quad (\text{S8})$$

with the unit vector  $\hat{m} \in \mathbb{R}^D$ . The generator is assumed to be a linear collective spin operator

$$\hat{G} = \hat{J}_{\hat{n}} = \hat{n} \cdot \hat{\mathbf{J}} \quad (\text{S9})$$

in the direction  $\hat{n} \in \mathbb{R}^3$  with the family of linear collective spin operators

$$\hat{\mathbf{J}} \equiv (\hat{J}_x, \hat{J}_y, \hat{J}_z). \quad (\text{S10})$$

Thus, the optimal metrological squeezing parameter for this family of operators can be written as

$$\xi_{\text{opt}}^2[\rho, \hat{\mathbf{S}}] = \min_{\hat{X} \in \text{span}(\hat{\mathbf{S}})} \min_{\hat{G} \in \text{span}(\hat{\mathbf{J}})} \xi^2[\rho, \hat{X}, \hat{G}] = \min_{\hat{m} \in \mathbb{R}^D} \min_{\hat{n} \in \mathbb{R}^3} \frac{N(\Delta_\rho \hat{S}_{\hat{m}})^2}{|\langle [\hat{S}_{\hat{m}}, \hat{J}_{\hat{n}}] \rangle_\rho|^2} = \frac{N}{\lambda_{\max}(\tilde{\mathcal{M}}[\rho, \hat{\mathbf{S}}])}, \quad (\text{S11})$$

where the last equality [Eq. (4) in the main text] is proved in Ref. [38],  $N$  is the number of qubits, and  $\lambda_{\max}(\tilde{\mathcal{M}}[\rho, \hat{\mathbf{S}}])$  is the largest eigenvalue of a  $3 \times 3$  matrix  $\tilde{\mathcal{M}}[\rho, \hat{\mathbf{S}}]$ . The matrix  $\tilde{\mathcal{M}}[\rho, \hat{\mathbf{S}}]$  contains the first three rows and columns of a  $D \times D$  matrix as

$$\mathcal{M}[\rho, \hat{\mathbf{S}}] = \mathcal{C}^T[\rho, \hat{\mathbf{S}}] \mathcal{V}^{-1}[\rho, \hat{\mathbf{S}}] \mathcal{C}[\rho, \hat{\mathbf{S}}], \quad (\text{S12})$$

where  $\mathcal{V}[\rho, \hat{\mathbf{S}}]$  is the covariance matrix (symmetric,  $\mathcal{V}^T = \mathcal{V}$ ) with elements:

$$\mathcal{V}_{ij}[\rho, \hat{\mathbf{S}}] = \text{Cov}_\rho(\hat{S}_i, \hat{S}_j) = \frac{\langle \{\hat{S}_i, \hat{S}_j\} \rangle_\rho}{2} - \langle \hat{S}_i \rangle_\rho \langle \hat{S}_j \rangle_\rho, \quad (\text{S13})$$

and  $\mathcal{C}[\rho, \hat{\mathbf{H}}]$  is the real-valued skew-symmetric commutator matrix (asymmetric,  $\mathcal{C}^T = -\mathcal{C}$ ) with elements:

$$\mathcal{C}_{ij}[\rho, \hat{\mathbf{S}}] = -i \langle [\hat{S}_i, \hat{S}_j] \rangle_\rho. \quad (\text{S14})$$

## B. Linear Ramsey squeezing parameter

To optimize the linear Ramsey squeezing parameter using Eq. (S11), we consider the accessible operators as spanned by a family of collective spin operators

$$\hat{\mathbf{S}}_{(1)} \equiv \hat{\mathbf{J}} = (\hat{J}_x, \hat{J}_y, \hat{J}_z)_{D=3}. \quad (\text{S15})$$

Then, the optimal spin squeezed parameter can be calculated with matrices

$$\mathcal{V}_{(1)} = \begin{pmatrix} (\Delta_\rho \hat{J}_x)^2 & \text{cov}_\rho(\hat{J}_x, \hat{J}_y) & \text{cov}_\rho(\hat{J}_x, \hat{J}_z) \\ \vdots & (\Delta_\rho \hat{J}_y)^2 & \text{cov}_\rho(\hat{J}_y, \hat{J}_z) \\ \dots & \dots & (\Delta_\rho \hat{J}_z)^2 \end{pmatrix}, \quad (\text{S16})$$

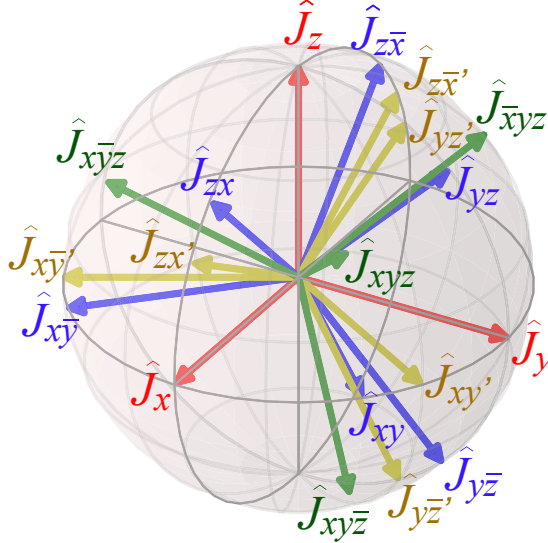


FIG. S4. Directions of collective spin operators for single-shot readout measurements. The collective spin operators to obtain the second-order nonlinear squeezing parameter via performing the single-shot readout measurement on each superconducting qubit:  $\{\hat{J}_x, \hat{J}_y, \hat{J}_z, \hat{J}_{xy}, \hat{J}_{yz}, \hat{J}_{zx}, \hat{J}_{xy}, \hat{J}_{yz}, \hat{J}_{zx}, \hat{J}_{xy'}, \hat{J}_{yz'}, \hat{J}_{zx'}, \hat{J}_{xy'}, \hat{J}_{yz'}, \hat{J}_{zx'}, \hat{J}_{xyz}, \hat{J}_{\bar{x}yz}, \hat{J}_{xy\bar{z}}\}$ , as shown in Eqs. (S22–S26). The unit vectors for the directions of these collective spin operators are plotted in a unit sphere.

$$\mathcal{C}_{(1)} = \begin{pmatrix} 0 & \langle \hat{J}_z \rangle_\rho & -\langle \hat{J}_y \rangle_\rho \\ -\langle \hat{J}_z \rangle_\rho & 0 & \langle \hat{J}_x \rangle_\rho \\ \langle \hat{J}_y \rangle_\rho & -\langle \hat{J}_x \rangle_\rho & 0 \end{pmatrix}, \quad (\text{S17})$$

where, e.g., the covariance  $\text{cov}_\rho(\hat{J}_x, \hat{J}_y)$  can be measured by the single-shot readout measurement of the observable operator  $\hat{J}_{xy} \equiv (\hat{J}_x + \hat{J}_y)/\sqrt{2}$  with

$$\text{cov}_\rho(\hat{J}_x, \hat{J}_y) = \langle \hat{J}_{xy}^2 \rangle_\rho - \frac{\langle \hat{J}_x^2 \rangle_\rho + \langle \hat{J}_y^2 \rangle_\rho}{2} - \langle \hat{J}_x \rangle_\rho \langle \hat{J}_y \rangle_\rho, \quad (\text{S18})$$

$$\text{cov}_\rho(\hat{J}_x, \hat{J}_z) = \langle \hat{J}_{xz}^2 \rangle_\rho - \frac{\langle \hat{J}_x^2 \rangle_\rho + \langle \hat{J}_z^2 \rangle_\rho}{2} - \langle \hat{J}_x \rangle_\rho \langle \hat{J}_z \rangle_\rho, \quad (\text{S19})$$

$$\text{cov}_\rho(\hat{J}_y, \hat{J}_z) = \langle \hat{J}_{yz}^2 \rangle_\rho - \frac{\langle \hat{J}_y^2 \rangle_\rho + \langle \hat{J}_z^2 \rangle_\rho}{2} - \langle \hat{J}_y \rangle_\rho \langle \hat{J}_z \rangle_\rho. \quad (\text{S20})$$

### C. Second-order nonlinear squeezing parameter

For the second-order nonlinear squeezing parameter, we introduce a family of  $D = 9$  linear and quadratic collective spin operators,

$$\hat{\mathbf{S}}_{(2)} = (\hat{J}_x, \hat{J}_y, \hat{J}_z, \hat{J}_x^2, \hat{J}_y^2, \hat{J}_z^2, \hat{J}_{xy}^2, \hat{J}_{yz}^2, \hat{J}_{zx}^2)_{D=9}, \quad (\text{S21})$$

with the single-shot readout measurements of the operators, as shown in Fig. S4 with direction vectors on a unit sphere.

$$\hat{J}_x, \quad \hat{J}_y, \quad \hat{J}_z \quad (\text{S22})$$

$$\hat{J}_{xy} = \frac{\hat{J}_x + \hat{J}_y}{\sqrt{2}}, \quad \hat{J}_{yz} = \frac{\hat{J}_y + \hat{J}_z}{\sqrt{2}}, \quad \hat{J}_{zx} = \frac{\hat{J}_x + \hat{J}_z}{\sqrt{2}}, \quad \hat{J}_{x\bar{y}} = \frac{\hat{J}_x - \hat{J}_y}{\sqrt{2}}, \quad \hat{J}_{y\bar{z}} = \frac{\hat{J}_y - \hat{J}_z}{\sqrt{2}}, \quad \hat{J}_{z\bar{x}} = \frac{\hat{J}_z - \hat{J}_x}{\sqrt{2}}, \quad (\text{S23})$$

$$\hat{J}_{xy'} = \frac{\hat{J}_x + \sqrt{3}\hat{J}_y}{2}, \quad \hat{J}_{yz'} = \frac{\hat{J}_y + \sqrt{3}\hat{J}_z}{2}, \quad \hat{J}_{zx'} = \frac{\hat{J}_z + \sqrt{3}\hat{J}_x}{2}, \quad (\text{S24})$$

$$\hat{J}_{x\bar{y}'} = \frac{\hat{J}_x - \sqrt{3}\hat{J}_y}{2}, \quad \hat{J}_{y\bar{z}'} = \frac{\hat{J}_y - \sqrt{3}\hat{J}_z}{2}, \quad \hat{J}_{z\bar{x}'} = \frac{\hat{J}_z - \sqrt{3}\hat{J}_x}{2}, \quad (\text{S25})$$

$$\hat{J}_{xyz} = \frac{\hat{J}_x + \hat{J}_y + \hat{J}_z}{\sqrt{3}}, \quad \hat{J}_{\bar{x}yz} = \frac{-\hat{J}_x + \hat{J}_y + \hat{J}_z}{\sqrt{3}}, \quad \hat{J}_{x\bar{y}z} = \frac{\hat{J}_x - \hat{J}_y + \hat{J}_z}{\sqrt{3}}, \quad \hat{J}_{x\bar{y}\bar{z}} = \frac{\hat{J}_x + \hat{J}_y - \hat{J}_z}{\sqrt{3}}. \quad (\text{S26})$$

The covariance matrix  $\mathcal{V}_{(2)}$  for the second-order spin squeezing parameter is written as

$$\mathcal{V}_{(2)} = \begin{pmatrix} \mathcal{V}_{(1)} & \left| \begin{array}{ccc} \text{cov}_\rho(J_x, J_x^2) & \text{cov}_\rho(\hat{J}_x, \hat{J}_y^2) & \text{cov}_\rho(\hat{J}_x, \hat{J}_z^2) \\ \text{cov}_\rho(\hat{J}_y, \hat{J}_x^2) & \text{cov}_\rho(\hat{J}_y, \hat{J}_y^2) & \text{cov}_\rho(\hat{J}_y, \hat{J}_z^2) \\ \text{cov}_\rho(\hat{J}_z, \hat{J}_x^2) & \text{cov}_\rho(\hat{J}_z, \hat{J}_y^2) & \text{cov}_\rho(\hat{J}_z, \hat{J}_z^2) \end{array} \right| \\ \hline \vdots & \left| \begin{array}{ccc} (\Delta_\rho \hat{J}_x^2)^2 & \text{cov}_\rho(\hat{J}_x^2, \hat{J}_y^2) & \text{cov}_\rho(\hat{J}_x^2, \hat{J}_z^2) \\ \vdots & (\Delta_\rho \hat{J}_y^2)^2 & \text{cov}_\rho(\hat{J}_y^2, \hat{J}_z^2) \\ \dots & \dots & (\Delta_\rho \hat{J}_z^2)^2 \end{array} \right| \\ \hline \vdots & \left| \begin{array}{ccc} (\Delta_\rho \hat{J}_{xy}^2)^2 & \text{cov}_\rho(\hat{J}_{xy}^2, \hat{J}_{yz}^2) & \text{cov}_\rho(\hat{J}_{xy}^2, \hat{J}_{zx}^2) \\ \vdots & (\Delta_\rho \hat{J}_{yz}^2)^2 & \text{cov}_\rho(\hat{J}_{yz}^2, \hat{J}_{zx}^2) \\ \dots & \dots & (\Delta_\rho \hat{J}_{zx}^2)^2 \end{array} \right| \end{pmatrix}, \quad (\text{S27})$$

with some of the elements being written in terms of the averages of measurable observables, as listed below: [We have shown the elements for the first three rows and columns in Eq. (S16).]

$$\text{cov}_\rho(\hat{J}_x^2, \hat{J}_y^2) = [2(\langle \hat{J}_{xy}^4 \rangle_\rho + \langle \hat{J}_{x\bar{y}}^4 \rangle_\rho) - \langle \hat{J}_x^4 \rangle_\rho - \langle \hat{J}_y^4 \rangle_\rho - 3\langle \hat{J}_z^2 \rangle_\rho + 2\langle \hat{J}_y^2 \rangle_\rho + 2\langle \hat{J}_x^2 \rangle_\rho]/6 - \langle \hat{J}_x^2 \rangle_\rho \langle \hat{J}_y^2 \rangle_\rho, \quad (\text{S28})$$

$$\text{cov}_\rho(\hat{J}_x^2, \hat{J}_z^2) = [2(\langle \hat{J}_{zx}^4 \rangle_\rho + \langle \hat{J}_{z\bar{x}}^4 \rangle_\rho) - \langle \hat{J}_x^4 \rangle_\rho - \langle \hat{J}_z^4 \rangle_\rho - 3\langle \hat{J}_y^2 \rangle_\rho + 2\langle \hat{J}_x^2 \rangle_\rho + 2\langle \hat{J}_z^2 \rangle_\rho]/6 - \langle \hat{J}_x^2 \rangle_\rho \langle \hat{J}_z^2 \rangle_\rho, \quad (\text{S29})$$

$$\text{cov}_\rho(\hat{J}_y^2, \hat{J}_z^2) = [2(\langle \hat{J}_{yz}^4 \rangle_\rho + \langle \hat{J}_{y\bar{z}}^4 \rangle_\rho) - \langle \hat{J}_y^4 \rangle_\rho - \langle \hat{J}_z^4 \rangle_\rho - 3\langle \hat{J}_x^2 \rangle_\rho + 2\langle \hat{J}_y^2 \rangle_\rho + 2\langle \hat{J}_z^2 \rangle_\rho]/6 - \langle \hat{J}_y \rangle_\rho \langle \hat{J}_z \rangle_\rho, \quad (\text{S30})$$

and

$$\text{cov}_\rho(\hat{J}_x, \hat{J}_y^2) = [\sqrt{2}(\langle \hat{J}_{xy}^3 \rangle_\rho + \langle \hat{J}_{x\bar{y}}^3 \rangle_\rho) - \langle \hat{J}_x^3 \rangle_\rho + \langle \hat{J}_x \rangle_\rho/2]/3 - \langle \hat{J}_x \rangle_\rho \langle \hat{J}_y^2 \rangle_\rho, \quad (\text{S31})$$

$$\text{cov}_\rho(\hat{J}_y, \hat{J}_z^2) = [\sqrt{2}(\langle \hat{J}_{yz}^3 \rangle_\rho + \langle \hat{J}_{y\bar{z}}^3 \rangle_\rho) - \langle \hat{J}_y^3 \rangle_\rho + \langle \hat{J}_y \rangle_\rho/2]/3 - \langle \hat{J}_y \rangle_\rho \langle \hat{J}_z^2 \rangle_\rho, \quad (\text{S32})$$

$$\text{cov}_\rho(\hat{J}_z, \hat{J}_x^2) = [\sqrt{2}(\langle \hat{J}_{zx}^3 \rangle_\rho + \langle \hat{J}_{z\bar{x}}^3 \rangle_\rho) - \langle \hat{J}_z^3 \rangle_\rho + \langle \hat{J}_z \rangle_\rho/2]/3 - \langle \hat{J}_z \rangle_\rho \langle \hat{J}_x^2 \rangle_\rho, \quad (\text{S33})$$

$$\text{cov}_\rho(\hat{J}_x, \hat{J}_z^2) = [\sqrt{2}(\langle \hat{J}_{xz}^3 \rangle_\rho - \langle \hat{J}_{z\bar{x}}^3 \rangle_\rho) - \langle \hat{J}_x^3 \rangle_\rho + \langle \hat{J}_x \rangle_\rho/2]/3 - \langle \hat{J}_x \rangle_\rho \langle \hat{J}_z^2 \rangle_\rho, \quad (\text{S34})$$

$$\text{cov}_\rho(\hat{J}_y, \hat{J}_x^2) = [\sqrt{2}(\langle \hat{J}_{xy}^3 \rangle_\rho - \langle \hat{J}_{x\bar{y}}^3 \rangle_\rho) - \langle \hat{J}_y^3 \rangle_\rho + \langle \hat{J}_y \rangle_\rho/2]/3 - \langle \hat{J}_y \rangle_\rho \langle \hat{J}_x^2 \rangle_\rho, \quad (\text{S35})$$

$$\text{cov}_\rho(\hat{J}_z, \hat{J}_y^2) = [\sqrt{2}(\langle \hat{J}_{yz}^3 \rangle_\rho - \langle \hat{J}_{y\bar{z}}^3 \rangle_\rho) - \langle \hat{J}_z^3 \rangle_\rho + \langle \hat{J}_z \rangle_\rho/2]/3 - \langle \hat{J}_z \rangle_\rho \langle \hat{J}_y^2 \rangle_\rho, \quad (\text{S36})$$





The skew-symmetric commutator matrix is written as

$$\mathcal{C} = -i \langle \begin{pmatrix} 0 & [\hat{J}_x, \hat{J}_y] & [\hat{J}_x, \hat{J}_z] & 0 & [\hat{J}_x, \hat{J}_y^2] & [\hat{J}_x, \hat{J}_z^2] & [\hat{J}_x, \hat{J}_{xy}] & [\hat{J}_x, \hat{J}_{yz}] & [\hat{J}_x, \hat{J}_{zx}] \\ 0 & [\hat{J}_y, \hat{J}_z] & [\hat{J}_y, \hat{J}_x^2] & 0 & [\hat{J}_y, \hat{J}_z^2] & [\hat{J}_y, \hat{J}_{xy}] & [\hat{J}_y, \hat{J}_{yz}] & [\hat{J}_y, \hat{J}_{zx}] \\ 0 & [\hat{J}_z, \hat{J}_x^2] & [\hat{J}_z, \hat{J}_y^2] & 0 & [\hat{J}_z, \hat{J}_x^2] & [\hat{J}_z, \hat{J}_{xy}] & [\hat{J}_z, \hat{J}_{yz}] & [\hat{J}_z, \hat{J}_{zx}] \\ \hline & 0 & [\hat{J}_x^2, \hat{J}_y^2] & [\hat{J}_x^2, \hat{J}_z^2] & 0 & [\hat{J}_x^2, \hat{J}_{xy}] & [\hat{J}_x^2, \hat{J}_{yz}] & [\hat{J}_x^2, \hat{J}_{zx}] \\ & & 0 & [\hat{J}_y^2, \hat{J}_z^2] & 0 & [\hat{J}_y^2, \hat{J}_{xy}] & [\hat{J}_y^2, \hat{J}_{yz}] & [\hat{J}_y^2, \hat{J}_{zx}] \\ & & & 0 & [\hat{J}_z^2, \hat{J}_{xy}] & [\hat{J}_z^2, \hat{J}_{yz}] & [\hat{J}_z^2, \hat{J}_{zx}] & [\hat{J}_z^2, \hat{J}_{xz}] \\ \hline & & & & 0 & [\hat{J}_{xy}^2, \hat{J}_{yz}^2] & [\hat{J}_{xy}^2, \hat{J}_{zx}^2] & 0 \\ & & & & & 0 & [\hat{J}_{yz}^2, \hat{J}_{zx}^2] & 0 \end{pmatrix} \rangle_{\rho}, \quad (\text{S58})$$

with elements

$$-i\langle[\hat{J}_x, \hat{J}_y]\rangle_{\rho} = \langle\hat{J}_z\rangle_{\rho}, \quad -i\langle[\hat{J}_x, \hat{J}_z]\rangle_{\rho} = -\langle\hat{J}_y\rangle_{\rho}, \quad -i\langle[\hat{J}_y, \hat{J}_z]\rangle_{\rho} = \langle\hat{J}_x\rangle_{\rho}, \quad (\text{S59})$$

$$-i\langle[\hat{J}_x, \hat{J}_y^2]\rangle_{\rho} = 2\langle\hat{J}_{yz}\rangle_{\rho} - \langle\hat{J}_y^2\rangle_{\rho} - \langle\hat{J}_z^2\rangle_{\rho}, \quad -i\langle[\hat{J}_x, \hat{J}_z^2]\rangle_{\rho} = 2\langle\hat{J}_{yz}\rangle_{\rho} - \langle\hat{J}_y^2\rangle_{\rho} - \langle\hat{J}_z^2\rangle_{\rho}, \quad (\text{S60})$$

$$-i\langle[\hat{J}_y, \hat{J}_z^2]\rangle_{\rho} = 2\langle\hat{J}_{zx}\rangle_{\rho} - \langle\hat{J}_z^2\rangle_{\rho} - \langle\hat{J}_x^2\rangle_{\rho}, \quad -i\langle[\hat{J}_y, \hat{J}_x^2]\rangle_{\rho} = 2\langle\hat{J}_{zx}\rangle_{\rho} - \langle\hat{J}_z^2\rangle_{\rho} - \langle\hat{J}_x^2\rangle_{\rho}, \quad (\text{S61})$$

$$-i\langle[\hat{J}_z, \hat{J}_x^2]\rangle_{\rho} = 2\langle\hat{J}_{xy}\rangle_{\rho} - \langle\hat{J}_x^2\rangle_{\rho} - \langle\hat{J}_y^2\rangle_{\rho}, \quad -i\langle[\hat{J}_z, \hat{J}_y^2]\rangle_{\rho} = 2\langle\hat{J}_{xy}\rangle_{\rho} - \langle\hat{J}_x^2\rangle_{\rho} - \langle\hat{J}_y^2\rangle_{\rho}, \quad (\text{S62})$$

and

$$-i\langle[\hat{J}_x^2, \hat{J}_y^2]\rangle_{\rho} = 2\sqrt{3}\langle\hat{J}_{xyz}\rangle_{\rho} - \frac{4\sqrt{2}(\langle\hat{J}_{xy}^3\rangle_{\rho} + \langle\hat{J}_{yz}^3\rangle_{\rho} + \langle\hat{J}_{zx}^3\rangle_{\rho})}{3} + \frac{2(\langle\hat{J}_x^3\rangle_{\rho} + \langle\hat{J}_y^3\rangle_{\rho} + \langle\hat{J}_z^3\rangle_{\rho})}{3}, \quad (\text{S63})$$

$$-i\langle[\hat{J}_x^2, \hat{J}_z^2]\rangle_{\rho} = i\langle[\hat{J}_x^2, \hat{J}_y^2]\rangle_{\rho}, \quad (\text{S64})$$

$$-i\langle[\hat{J}_y^2, \hat{J}_z^2]\rangle_{\rho} = -i\langle[\hat{J}_x^2, \hat{J}_y^2]\rangle_{\rho}, \quad (\text{S65})$$

to further obtain that

$$-i\langle[\hat{J}_x, \hat{J}_{xy}^2]\rangle_{\rho} = \frac{i}{2}\langle[\hat{J}_y, \hat{J}_x^2]\rangle_{\rho} - \frac{i}{2}\langle[\hat{J}_x, \hat{J}_y^2]\rangle_{\rho}, \quad -i\langle[\hat{J}_x, \hat{J}_{zx}^2]\rangle_{\rho} = \frac{i}{2}\langle[\hat{J}_z, \hat{J}_x^2]\rangle_{\rho} - \frac{i}{2}\langle[\hat{J}_x, \hat{J}_z^2]\rangle_{\rho}, \quad (\text{S66})$$

$$-i\langle[\hat{J}_y, \hat{J}_{xy}^2]\rangle_{\rho} = \frac{i}{2}\langle[\hat{J}_x, \hat{J}_y^2]\rangle_{\rho} - \frac{i}{2}\langle[\hat{J}_y, \hat{J}_x^2]\rangle_{\rho}, \quad -i\langle[\hat{J}_y, \hat{J}_{yz}^2]\rangle_{\rho} = \frac{i}{2}\langle[\hat{J}_z, \hat{J}_y^2]\rangle_{\rho} - \frac{i}{2}\langle[\hat{J}_y, \hat{J}_z^2]\rangle_{\rho}, \quad (\text{S67})$$

$$-i\langle[\hat{J}_z, \hat{J}_{yz}^2]\rangle_{\rho} = \frac{i}{2}\langle[\hat{J}_y, \hat{J}_z^2]\rangle_{\rho} - \frac{i}{2}\langle[\hat{J}_z, \hat{J}_y^2]\rangle_{\rho}, \quad -i\langle[\hat{J}_z, \hat{J}_{zx}^2]\rangle_{\rho} = \frac{i}{2}\langle[\hat{J}_x, \hat{J}_z^2]\rangle_{\rho} - \frac{i}{2}\langle[\hat{J}_z, \hat{J}_x^2]\rangle_{\rho}, \quad (\text{S68})$$

and

$$-i\langle[\hat{J}_x, \hat{J}_{yz}^2]\rangle_{\rho} = -\frac{i}{2}\langle[\hat{J}_x, \hat{J}_y^2]\rangle_{\rho} - \frac{i}{2}\langle[\hat{J}_x, \hat{J}_z^2]\rangle_{\rho} + \langle\hat{J}_z^2\rangle_{\rho} - \langle\hat{J}_y^2\rangle_{\rho}, \quad (\text{S69})$$

$$-i\langle[\hat{J}_y, \hat{J}_{zx}^2]\rangle_{\rho} = -\frac{i}{2}\langle[\hat{J}_y, \hat{J}_z^2]\rangle_{\rho} - \frac{i}{2}\langle[\hat{J}_y, \hat{J}_x^2]\rangle_{\rho} + \langle\hat{J}_x^2\rangle_{\rho} - \langle\hat{J}_z^2\rangle_{\rho}, \quad (\text{S70})$$

$$-i\langle[\hat{J}_z, \hat{J}_{xy}^2]\rangle_{\rho} = -\frac{i}{2}\langle[\hat{J}_z, \hat{J}_x^2]\rangle_{\rho} - \frac{i}{2}\langle[\hat{J}_z, \hat{J}_y^2]\rangle_{\rho} + \langle\hat{J}_y^2\rangle_{\rho} - \langle\hat{J}_x^2\rho, \quad (\text{S71})$$

and

$$-i\langle[\hat{J}_x^2, \hat{J}_{xy}^2]\rangle_{\rho} = \frac{2\sqrt{2}(\langle\hat{J}_{zx}^3\rangle_{\rho} + \langle\hat{J}_{xz}^3\rangle_{\rho})}{3} - \frac{2\langle\hat{J}_{xy}^3\rangle_{\rho}}{3} - \frac{\langle\hat{J}_z\rangle_{\rho}}{6} - \frac{i}{2}\langle[\hat{J}_x^2, \hat{J}_y^2]\rangle_{\rho}, \quad (\text{S72})$$

$$-i\langle[\hat{J}_y^2, \hat{J}_{yz}^2]\rangle_{\rho} = \frac{2\sqrt{2}(\langle\hat{J}_{xy}^3\rangle_{\rho} + \langle\hat{J}_{xy}^3\rangle_{\rho})}{3} - \frac{2\langle\hat{J}_x^3\rangle_{\rho}}{3} - \frac{\langle\hat{J}_x\rangle_{\rho}}{6} - \frac{i}{2}\langle[\hat{J}_y^2, \hat{J}_z^2]\rangle_{\rho}, \quad (\text{S73})$$

$$-i\langle[\hat{J}_z^2, \hat{J}_{zx}^2]\rangle_{\rho} = \frac{2\sqrt{2}(\langle\hat{J}_{yz}^3\rangle_{\rho} + \langle\hat{J}_{yz}^3\rangle_{\rho})}{3} - \frac{2\langle\hat{J}_y^3\rangle_{\rho}}{3} - \frac{\langle\hat{J}_y\rangle_{\rho}}{6} - \frac{i}{2}\langle[\hat{J}_z^2, \hat{J}_x^2]\rangle_{\rho}, \quad (\text{S74})$$

$$-i\langle[\hat{J}_x^2, \hat{J}_{zx}^2]\rangle_{\rho} = -\frac{2\sqrt{2}(\langle\hat{J}_{xy}^3\rangle_{\rho} - \langle\hat{J}_{xy}^3\rangle_{\rho})}{3} + \frac{2\langle\hat{J}_{xy}^3\rangle_{\rho}}{3} + \frac{\langle\hat{J}_y\rangle_{\rho}}{6} - \frac{i}{2}\langle[\hat{J}_x^2, \hat{J}_z^2]\rangle_{\rho}, \quad (\text{S75})$$

$$-i\langle[\hat{J}_y^2, \hat{J}_{xy}^2]\rangle_{\rho} = -\frac{2\sqrt{2}(\langle\hat{J}_{yz}^3\rangle_{\rho} - \langle\hat{J}_{yz}^3\rangle_{\rho})}{3} + \frac{2\langle\hat{J}_z^3\rangle_{\rho}}{3} + \frac{\langle\hat{J}_z\rangle_{\rho}}{6} - \frac{i}{2}\langle[\hat{J}_y^2, \hat{J}_x^2]\rangle_{\rho}, \quad (\text{S76})$$

$$-i\langle[\hat{J}_z^2, \hat{J}_{yz}^2]\rangle_{\rho} = -\frac{2\sqrt{2}(\langle\hat{J}_{zx}^3\rangle_{\rho} - \langle\hat{J}_{zx}^3\rangle_{\rho})}{3} + \frac{2\langle\hat{J}_x^3\rangle_{\rho}}{3} + \frac{\langle\hat{J}_x\rangle_{\rho}}{6} - \frac{i}{2}\langle[\hat{J}_z^2, \hat{J}_y^2]\rangle_{\rho}, \quad (\text{S77})$$

and

$$-i\langle[\hat{J}_x^2, \hat{J}_{yz}^2]\rangle_\rho = \frac{2\sqrt{2}(\langle\hat{J}_{zx}^3\rangle_\rho - \langle\hat{J}_{z\bar{x}}^3\rangle_\rho - \langle\hat{J}_{xy}^3\rangle_\rho - \langle\hat{J}_{x\bar{y}}^3\rangle_\rho)}{3} - \frac{i}{2}\langle[\hat{J}_x^2, \hat{J}_y^2]\rangle_\rho - \frac{i}{2}\langle[\hat{J}_x^2, \hat{J}_z^2]\rangle_\rho, \quad (\text{S78})$$

$$-i\langle[\hat{J}_y^2, \hat{J}_{zx}^2]\rangle_\rho = \frac{2\sqrt{2}(\langle\hat{J}_{xy}^3\rangle_\rho - \langle\hat{J}_{x\bar{y}}^3\rangle_\rho - \langle\hat{J}_{yz}^3\rangle_\rho - \langle\hat{J}_{y\bar{z}}^3\rangle_\rho)}{3} - \frac{i}{2}\langle[\hat{J}_y^2, \hat{J}_x^2]\rangle_\rho - \frac{i}{2}\langle[\hat{J}_y^2, \hat{J}_z^2]\rangle_\rho, \quad (\text{S79})$$

$$-i\langle[\hat{J}_z^2, \hat{J}_{xy}^2]\rangle_\rho = \frac{2\sqrt{2}(\langle\hat{J}_{yz}^3\rangle_\rho - \langle\hat{J}_{y\bar{z}}^3\rangle_\rho - \langle\hat{J}_{zx}^3\rangle_\rho - \langle\hat{J}_{z\bar{x}}^3\rangle_\rho)}{3} - \frac{i}{2}\langle[\hat{J}_z^2, \hat{J}_x^2]\rangle_\rho - \frac{i}{2}\langle[\hat{J}_z^2, \hat{J}_y^2]\rangle_\rho, \quad (\text{S80})$$

then to further obtain that

$$\begin{aligned} -i\langle[\hat{J}_{xy}^2, \hat{J}_{yz}^2]\rangle_\rho &= \frac{-i\langle[\hat{J}_x^2, \hat{J}_{yz}^2]\rangle_\rho - i\langle[\hat{J}_y^2, \hat{J}_{yz}^2]\rangle_\rho + i\langle[\hat{J}_y^2, \hat{J}_{xy}^2]\rangle_\rho + i\langle[\hat{J}_z^2, \hat{J}_{xy}^2]\rangle_\rho}{2} + \frac{i\langle[\hat{J}_x^2, \hat{J}_y^2]\rangle_\rho + i\langle[\hat{J}_x^2, \hat{J}_z^2]\rangle_\rho + i\langle[\hat{J}_y^2, \hat{J}_z^2]\rangle_\rho}{4} \\ &\quad + \text{cov}_\rho(\hat{J}_y, \hat{J}_z + \hat{J}_x) - \langle\hat{J}_y^3\rangle_\rho - \frac{\langle\hat{J}_y\rangle_\rho}{4} + \langle\hat{J}_y\rangle_\rho(\langle\hat{J}_z^2\rangle_\rho + \langle\hat{J}_x^2\rangle_\rho), \end{aligned} \quad (\text{S81})$$

$$\begin{aligned} -i\langle[\hat{J}_{xy}^2, \hat{J}_{zx}^2]\rangle_\rho &= \frac{-i\langle[\hat{J}_x^2, \hat{J}_{zx}^2]\rangle_\rho - i\langle[\hat{J}_y^2, \hat{J}_{zx}^2]\rangle_\rho + i\langle[\hat{J}_z^2, \hat{J}_{xy}^2]\rangle_\rho + i\langle[\hat{J}_x^2, \hat{J}_{xy}^2]\rangle_\rho}{2} + \frac{i\langle[\hat{J}_x^2, \hat{J}_z^2]\rangle_\rho + i\langle[\hat{J}_y^2, \hat{J}_z^2]\rangle_\rho + i\langle[\hat{J}_y^2, \hat{J}_x^2]\rangle_\rho}{4} \\ &\quad - \text{cov}_\rho(\hat{J}_x, \hat{J}_y + \hat{J}_z) + \langle\hat{J}_x^3\rangle_\rho + \frac{\langle\hat{J}_x\rangle_\rho}{4} - \langle\hat{J}_x\rangle_\rho(\langle\hat{J}_y^2\rangle_\rho + \langle\hat{J}_z^2\rangle_\rho), \end{aligned} \quad (\text{S82})$$

$$\begin{aligned} -i\langle[\hat{J}_{yz}^2, \hat{J}_{zx}^2]\rangle_\rho &= \frac{-i\langle[\hat{J}_y^2, \hat{J}_{zx}^2]\rangle_\rho - i\langle[\hat{J}_z^2, \hat{J}_{zx}^2]\rangle_\rho + i\langle[\hat{J}_x^2, \hat{J}_{yz}^2]\rangle_\rho + i\langle[\hat{J}_z^2, \hat{J}_{yz}^2]\rangle_\rho}{2} + \frac{i\langle[\hat{J}_y^2, \hat{J}_z^2]\rangle_\rho + i\langle[\hat{J}_y^2, \hat{J}_x^2]\rangle_\rho + i\langle[\hat{J}_z^2, \hat{J}_x^2]\rangle_\rho}{4} \\ &\quad + \text{cov}_\rho(\hat{J}_z, \hat{J}_x + \hat{J}_y) - \langle\hat{J}_z^3\rangle_\rho - \frac{\langle\hat{J}_z\rangle_\rho}{4} + \langle\hat{J}_z\rangle_\rho(\langle\hat{J}_x^2\rangle_\rho + \langle\hat{J}_y^2\rangle_\rho). \end{aligned} \quad (\text{S83})$$

#### D. Efficient detection of second-order nonlinear squeezing parameter with seven operators

In our experiments, to obtain the nonlinear squeezing parameter, we select seven collective spin operators,

$$\hat{\mathbf{S}}_{\text{exp}} = (\hat{J}_x, \hat{J}_y, \hat{J}_z, \hat{J}_x^2, \hat{J}_y^2, \hat{J}_{xy}^2, \hat{J}_{zx}^2), \quad (\text{S84})$$

instead of the full family of the collective spin operators

$$\hat{\mathbf{S}}_{(2)} = (\hat{J}_x, \hat{J}_y, \hat{J}_z, \hat{J}_x^2, \hat{J}_y^2, \hat{J}_z^2, \hat{J}_{xy}^2, \hat{J}_{yz}^2, \hat{J}_{zx}^2), \quad (\text{S85})$$

for the second-order squeezing parameter [38]. As shown in Fig. 2(d) in the main text, we monitor the evolution of the nonlinear squeezing parameter via measuring each element of  $\mathcal{V}[\rho_t, \hat{\mathbf{S}}_{\text{exp}}]$  and  $\mathcal{C}[\rho_t, \hat{\mathbf{S}}_{\text{exp}}]$  (submatrices of  $\mathcal{V}[\rho_t, \hat{\mathbf{S}}_{(2)}]$  and  $\mathcal{C}[\rho_t, \hat{\mathbf{S}}_{(2)}]$ ) with simultaneous single-shot readouts of 10 qubits in different directions (see Fig. S4). The numerical simulations of the inverse nonlinear squeezing parameters,  $\xi_{\text{NL}}^{-2}[\rho_t, \hat{\mathbf{S}}_{(2)}]$  and  $\xi_{\text{NL}}^{-2}[\rho_t, \hat{\mathbf{S}}_{\text{exp}}]$  with respect to  $\hat{\mathbf{S}}_{(2)}$  and  $\hat{\mathbf{S}}_{\text{exp}}$ , respectively, are compared in Fig. S5. It is shown that the nonlinear squeezing parameter  $\xi_{\text{NL}}^{-2}[\rho_t, \hat{\mathbf{S}}_{\text{exp}}]$  with 7 selected collective spin operators is very close to the second-order nonlinear squeezing parameter  $\xi_{\text{NL}}^2[\rho_t, \hat{\mathbf{S}}_{\text{exp}}]$  for  $t \lesssim 76$  ns, and moreover, its minimum value is close to that of the  $\xi_{\text{NL}}^2[\rho_t, \hat{\mathbf{S}}_{(2)}]$ . Therefore, when choosing these 7 collective spin operators, we can efficiently detect the second-order nonlinear squeezing parameter with fewer observables to be measured. At  $t = 2$  ns, 34 ns, and 50 ns, the experimental results of matrices  $\mathcal{C}[\rho_t, \hat{\mathbf{S}}_{\text{exp}}]$ ,  $\mathcal{V}[\rho_t, \hat{\mathbf{S}}_{\text{exp}}]$ , and  $\mathcal{M}[\rho_t, \hat{\mathbf{S}}_{\text{exp}}]$  are compared with numerical simulations in Figs. S6, S7, and S8, respectively.

In addition, the method to optimize the squeezing parameter, based on searching for the largest eigenvalue of the matrix  $\mathcal{M}$  [38], requires a large number of trials of single-shot readouts for 19 observables (see Fig. S4) to obtain a reliable value of the second-order squeezing parameter. Thus, choosing 7 collective spin operators instead of 9 operators in our experiments can significantly reduce the number of readouts, and almost detect the large sensitivity enhancement for quantum metrology, which is characterized by the second-order nonlinear squeezing parameter with 9 operators.

#### E. Experimental details on measurement of squeezing parameters

In Fig. 2(d) of the main text, to calculate the linear spin squeezing parameter  $\xi_R^2$  at each time point  $t$ , we apply the experimental sequence shown in Fig. 1(d) of the main text, which is divided into four successive steps:

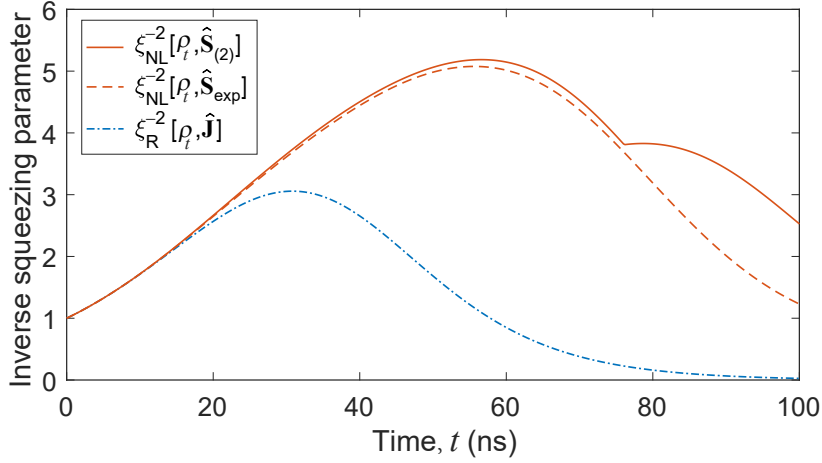


FIG. S5. Efficient detection of second-order nonlinear squeezing parameter with seven operators. Numerical simulations of the evolutions of the inverse Ramsey squeezing parameter,  $\xi_R^{-2}[\rho_t, \hat{J}]$ , with a family of 3 collective spin operators  $\hat{J} = (\hat{J}_x, \hat{J}_y, \hat{J}_z)$ , the inverse second-order nonlinear squeezing parameter,  $\xi_{NL}^{-2}[\rho_t, \hat{S}_{(2)}]$ , with 9 operators in Eq. (S85), and the inverse nonlinear squeezing parameter,  $\xi_{NL}^{-2}[\rho_t, \hat{S}_{exp}]$  with 7 operators in Eq. (S84).

- (i) The state preparation realized by  $Y_{\frac{\pi}{2}}$  gates.
- (ii) The nonlinear evolution where all qubits are equally detuned.
- (iii) The rotation pulses to measure qubits at different directions.
- (iv) The final joint single-shot readout.

We performed experimental runs repetitively for about 200,000 times in total for each linear collective spin operator,  $\hat{J}_\beta$ , listed in Eqs. (S22–S26). We then divided the results into 80 groups. For each group with  $i = 1, 2, \dots, 80$  denoting the group index, we obtain the joint raw probabilities of 10 qubits

$$\mathcal{P}_\beta^{(i)} = \{P_{0\dots 00}, P_{0\dots 01}, P_{0\dots 10}, \dots, P_{1\dots 11}\}, \quad (S86)$$

and then perform the readout correction on them to obtain the corrected probability,  $\tilde{\mathcal{P}}_\beta^{(i)}$ , after which the average of the observable,  $\langle \hat{J}_\beta \rangle_{\rho_t}^{(i)}$ , can be calculated for each group. Following the same process described above, we collect results for all the observables,  $\{\hat{J}_\beta\}$ , and calculate the linear Ramsey squeezing parameter,  $[\xi_R^2]^{(i)}$ , using Eq. (4) in the main text. The mean value and error bar of the  $\xi_R^2$  are estimated from these 80 groups of experimental data.

For the second-order nonlinear squeezing parameter,  $\xi_{NL}^2$ , as it requires a much larger number of experimental repetitions to become stable, which is time-consuming, we adopt a different method to estimate the error bar. From 84 groups of experimental data in total, we randomly select 40 groups of them and average these selected data (as a group labeled by  $j$ ) to calculate the second-order nonlinear squeezing parameter,  $[\xi_{NL}^2]^{(j)}$ . After repeating this process 10 times ( $j = 1, 2, \dots, 10$ ), we are able to estimate the error bar of the second-order nonlinear squeezing parameter by calculating the standard deviation of  $\{[\xi_{NL}^2]^{(1)}, [\xi_{NL}^2]^{(2)}, \dots, [\xi_{NL}^2]^{(10)}\}$ .

#### F. Observables for the optimal metrological squeezing parameters

By experimentally measuring the matrices  $\mathcal{V}$  and  $\mathcal{C}$ , the observable for the optimal metrological squeezing parameter can be obtained as

$$\hat{S}_{opt} = \hat{m}_{opt} \cdot \hat{S}, \quad (S87)$$

where

$$\hat{m}_{opt} = \mathcal{V}^{-1} \mathcal{C} \hat{m}', \quad (S88)$$

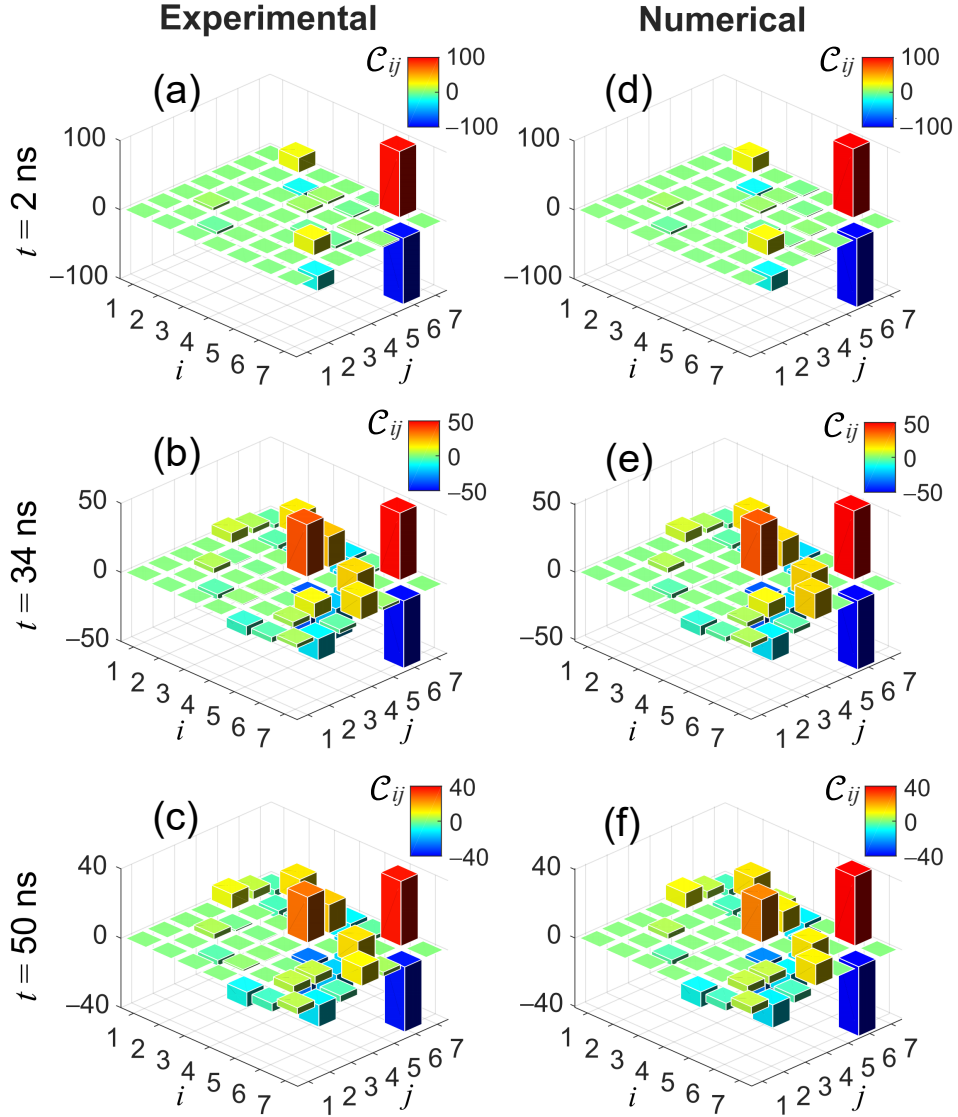


FIG. S6. Data of the  $\mathcal{C}$  matrix. (a–f) Matrix  $\mathcal{C}[\rho_t, \hat{\mathbf{S}}_{\text{exp}}]$  experimentally measured at (a)  $t = 2$  ns, (b)  $t = 34$  ns, and (c)  $t = 50$  ns, compared with the numerical simulations (d), (e), and (f).

and

$$\hat{m}' = (n'_1, n'_2, n'_3, 0, \dots, 0), \quad (\text{S89})$$

with  $\hat{n}_{\max} = (n'_1, n'_2, n'_3)$  being the eigenvector for the maximum eigenvalue of  $\hat{\mathcal{M}}[\rho, \hat{\mathbf{S}}]$  [38].

Benefiting from the nonlinear spin operators, i.e.,  $\hat{J}_x^2$ ,  $\hat{J}_y^2$ ,  $\hat{J}_{xy}^2$ , and  $\hat{J}_{zx}^2$ , the enhancement of metrological sensitivity is shown by the ratio of the inverse nonlinear squeezing parameter to the inverse linear squeezing parameter,  $\xi_{\text{NL}}^{-2}/\xi_{\text{R}}^{-2}$ , see Fig. S9(a). Extracted from the experimental data, the optimal observables for the linear squeezing parameter and the nonlinear squeezing parameter are shown in Fig. S9(b) and S9(c), respectively, which are compared with theoretical predictions.

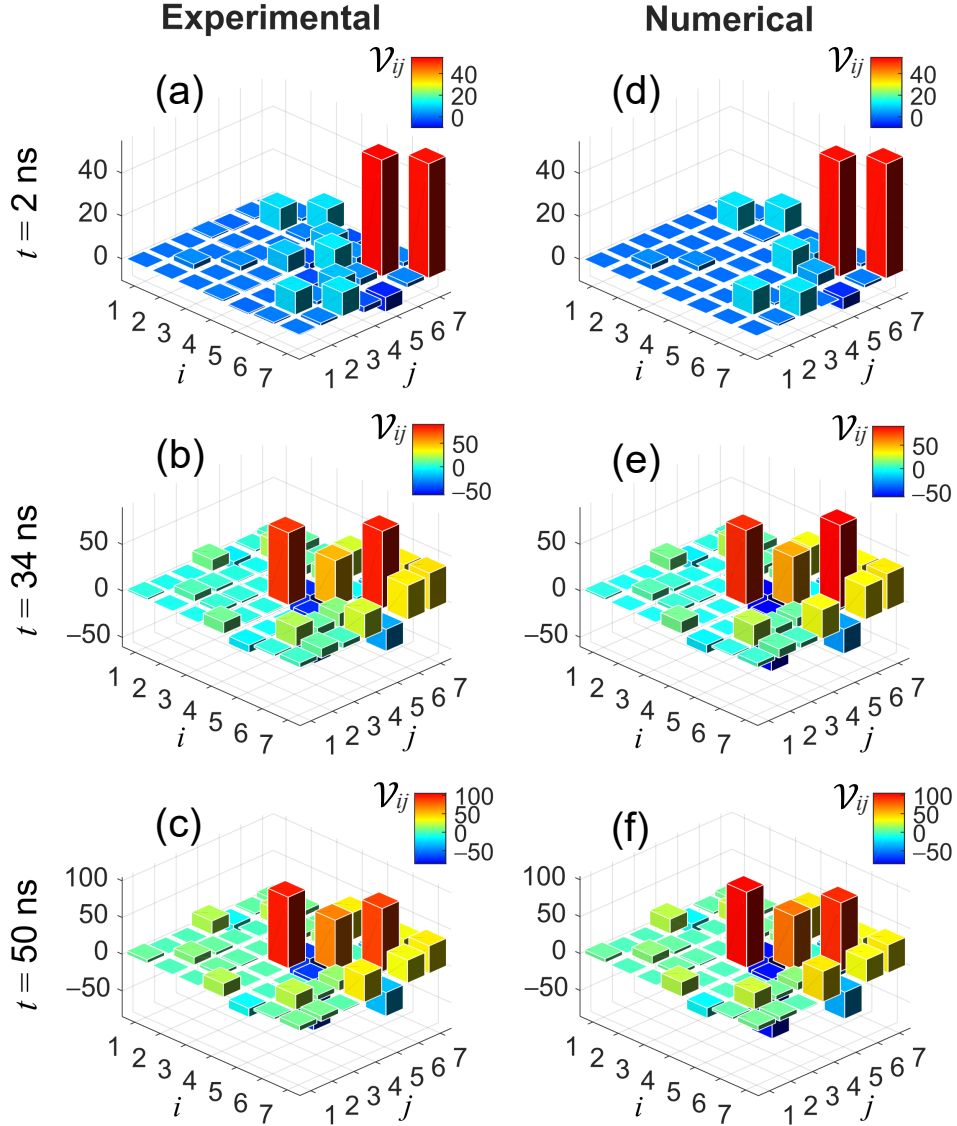


FIG. S7. Data of the  $\mathcal{V}$  matrix. (a–f) Matrix  $\mathcal{V}[\rho_t, \hat{\mathbf{S}}_{\text{exp}}]$  experimentally measured at (a)  $t = 2 \text{ ns}$ , (b)  $t = 34 \text{ ns}$ , and (c)  $t = 50 \text{ ns}$ , compared with the numerical simulations (d), (e), and (f).

## V. EXTRACTION OF THE FISHER INFORMATION

### A. Extraction of the Fisher information from the squared Hellinger distance

Given the generator,  $\hat{J}_y \equiv \sum_{j=1}^N \hat{\sigma}_j^y / 2$ , followed by an optimal angle,  $\alpha_{\text{opt}}$ , of the rotation along the  $x$ -axis to maximize the Fisher information, we imprint the phase  $\theta$  on the state as

$$\tilde{\rho}_t(\theta) = \exp(-i\hat{J}_y\theta) \exp(-i\hat{J}_x\alpha_{\text{opt}})\rho_t \exp(i\hat{J}_x\alpha_{\text{opt}}) \exp(i\hat{J}_y\theta), \quad (\text{S90})$$

and measure each superconducting qubit by the single-shot readout measurement to obtain the probability distribution of the observable  $\hat{J}_z \equiv \sum_{j=1}^N \hat{\sigma}_j^z / 2$ . To extract the Fisher information [39], we consider the squared Hellinger distance as

$$d_{\text{H}}^2(\theta) = 1 - \mathcal{F}_{\text{C}}[\{P_z(0)\}, \{P_z(\theta)\}] = 1 - \sum_z \sqrt{P_z(0)P_z(\theta)}, \quad (\text{S91})$$

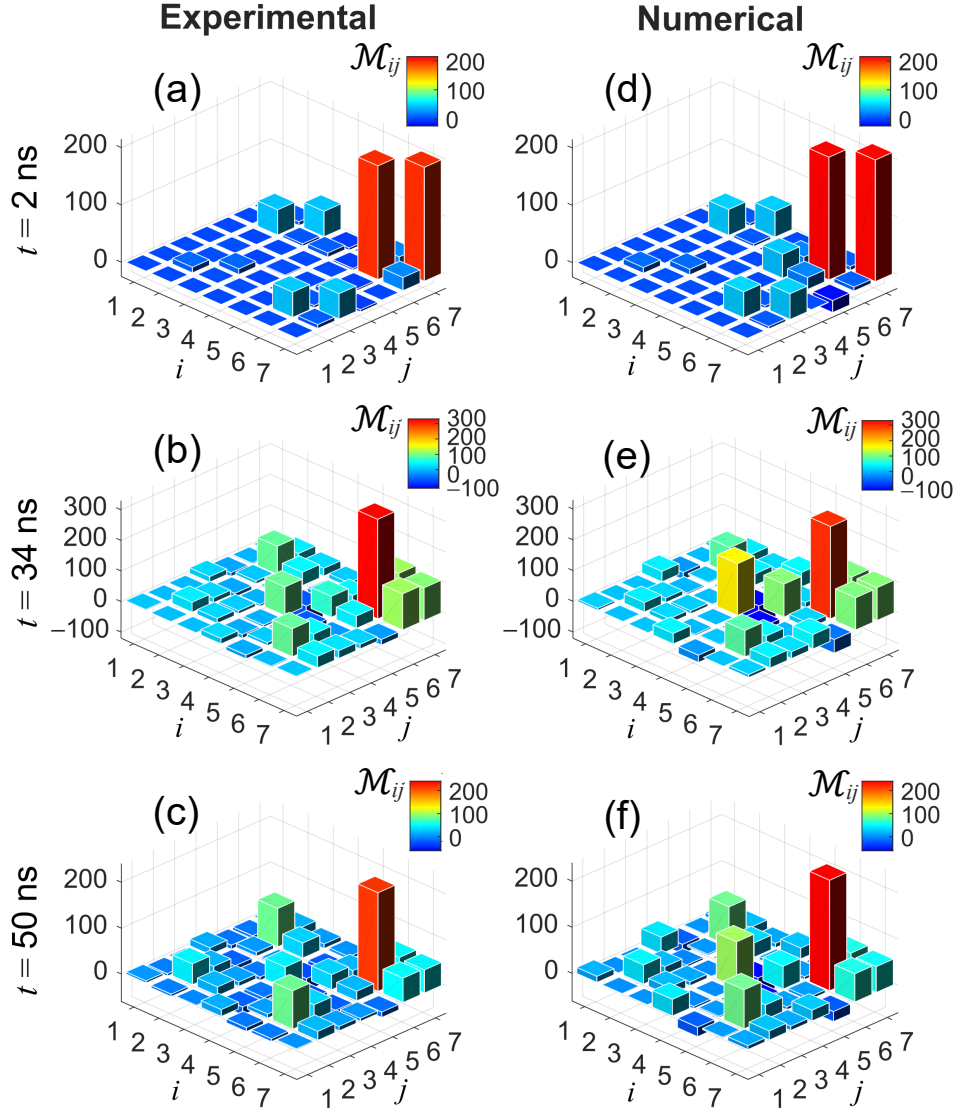


FIG. S8. Data of the  $\mathcal{M}$  matrix. (a–f) Matrix  $\mathcal{M}[\rho_t, \hat{\mathbf{S}}_{\text{exp}}]$  experimentally measured at (a)  $t = 2 \text{ ns}$ , (b)  $t = 34 \text{ ns}$ , and (c)  $t = 50 \text{ ns}$ , compared with the numerical simulations (d), (e), and (f).

where the Bhattacharyya coefficient (classical fidelity) is written as

$$\mathcal{F}_C[\{P_z(0)\}, \{P_z(\theta)\}] = \sum_z \sqrt{P_z(0)P_z(\theta)}, \quad (\text{S92})$$

with  $P_z(\theta)$  being the probability distribution of the output  $z = -\frac{N}{2}, -\frac{N}{2} + 1, \dots, \frac{N}{2} - 1, \frac{N}{2}$  of the observable  $\hat{J}_z$ . For a small  $\theta \rightarrow 0$ , the Taylor expansion of the squared Hellinger distance is given as [36]

$$d_H^2(\theta) = \frac{F(0)}{8}\theta^2 + \mathcal{O}(\theta^3), \quad (\text{S93})$$

where the Fisher information (divided by 8) can be regarded as the square of the speed of the Hellinger distance

$$\sqrt{F(0)/8} = v_H \equiv \left. \frac{\partial d_H(\theta)}{\partial \theta} \right|_{\theta=0}. \quad (\text{S94})$$

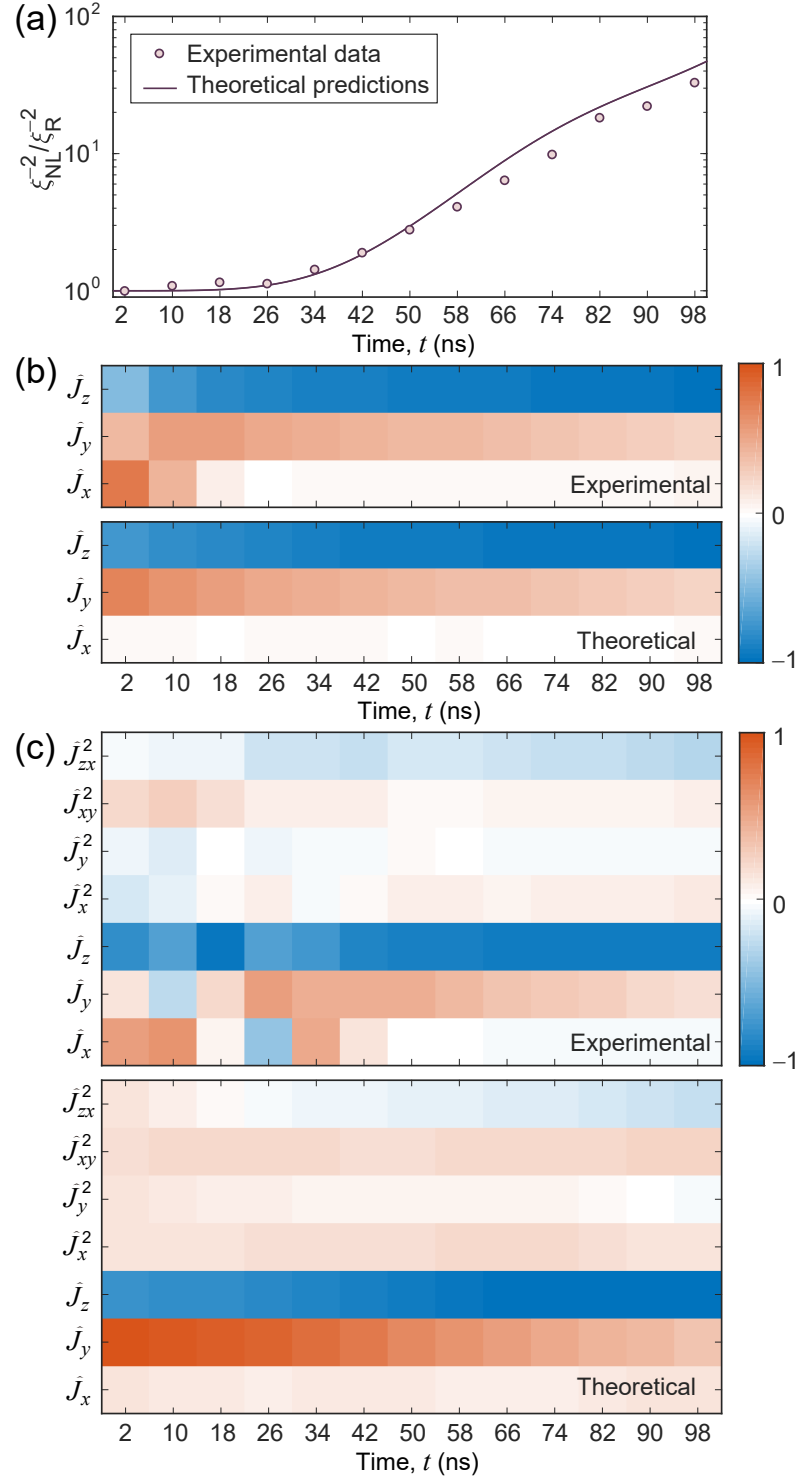


FIG. S9. (a) Time evolution of the ratio of the inverse nonlinear squeezing parameter to the inverse linear Ramsey squeezing parameter,  $\xi_{\text{NL}}^{-2}/\xi_{\text{R}}^{-2}$ . (b) The optimal observable (after normalization) for the linear Ramsey squeezing parameter, compared with the theoretical predictions, versus time  $t$ . (c) The optimal observable (after normalization) for the nonlinear squeezing parameter, compared with the theoretical predictions, versus time  $t$ .

In theory, by maximizing the squared Hellinger distance over all possible positive operator-valued measures (POVMs)  $\{\hat{E}\}$ , the squared Bures distance can be obtained

$$d_B^2(\theta) = \max_{\{\hat{E}\}} d_H^2(\theta) = 1 - \mathcal{F}_Q[\tilde{\rho}_t(0), \tilde{\rho}_t(\theta)], \quad (\text{S95})$$

where the Bures fidelity (quantum fidelity) between two states  $\rho(0)$  and  $\rho(\theta)$  reads

$$\mathcal{F}_Q[\tilde{\rho}_t(0), \tilde{\rho}_t(\theta)] \equiv \text{Tr}[\sqrt{\sqrt{\tilde{\rho}_t(0)}\tilde{\rho}_t(\theta)\sqrt{\tilde{\rho}_t(0)}}]. \quad (\text{S96})$$

The Taylor expansion of the squared Bures distance for  $\theta \rightarrow 0$  is given as [40]

$$d_B^2(\theta) = \frac{F_Q[\tilde{\rho}_t(0)]}{8}\theta^2 + \mathcal{O}(\theta^3) \quad (\text{S97})$$

where the quantum Fisher information (divided by 8) can be regarded as the square of the speed of the Bures distance

$$\sqrt{F_Q[\tilde{\rho}_t(0)]/8} = v_B \equiv \left. \frac{\partial d_B(\theta)}{\partial \theta} \right|_{\theta=0}, \quad (\text{S98})$$

and gives an achievable upper bound for the Fisher information for the optimal choice of the POVMs

$$F_Q[\tilde{\rho}_t(0)] = \max_{\{\hat{E}\}} F(0). \quad (\text{S99})$$

## B. Experimental details for extracting the Fisher information

In Fig. 4 of the main text, to obtain the Fisher information at time  $t$ , we apply the experimental sequence in Fig. 3(a), which successively includes: (i) the state preparation pulse  $Y_{\frac{\pi}{2}}$ , (ii) the nonlinear evolution  $\exp(-i\hat{H}t)$ , (iii) the optimization rotation  $X_\alpha$ , and (iv) the joint readouts in cases with and without the phase pulse  $Y_\theta$  inserted before the readouts. For each  $\theta$  and  $\alpha$ , we obtain the joint readout probabilities of 19 qubits

$$\mathcal{P}(\theta, \alpha) = \{P_{0...00}, P_{0...01}, P_{0...10}, \dots, P_{1...11}\}, \quad (\text{S100})$$

from which the probabilities  $\{P_z(\theta, \alpha)\}$  are extracted after performing the readout correction on  $\mathcal{P}(\theta, \alpha)$ . The Fisher information  $F(\theta = 0, \alpha)$  for different  $\alpha$  can then be extracted from the squared Hellinger distance of two states with and without the phase pulse  $Y_\theta$  inserted before the readouts using

$$F(0, \alpha) \simeq \frac{8 \times d_H^2(\theta, \alpha)}{\theta^2}, \quad (\text{S101})$$

with  $\theta$  being selected as a small value ( $-0.05$  rad in our experiment). The quadratic curve fitting of the square of the Hellinger distance versus the phase [Fig. 4(a) in the main text] fits the experimental data well for a relative small phase.

The optimized Fisher information is saturated by the optimal tomography angle  $\alpha_{\text{opt}}$  along the  $x$ -axis

$$F_{\text{opt}}(0) = \max_{\alpha} [F(0, \alpha)]. \quad (\text{S102})$$

To estimate the error bar, we perform about 600,000 experimental runs and obtain about 240 groups of the probabilities  $\{P_z(\theta, \alpha)\}^{(i)}$  for each  $\alpha$  and  $\theta$ , where  $i$  denotes the group index. After performing the readout correction on these probabilities, we randomly select 60 groups of them to calculate the Fisher information using the method described above. We repeat this random sampling process 10 times to calculate the final error bar of the Fisher information. Note that for  $t = 48$  ns, we only obtained 180 groups of probabilities from about 400,000 repetitive experimental runs in total, and we randomly selected 40 groups of them to calculate the error bar.

- [1] C. A. Sackett, D. Kielpinski, B. E. King, C. Langer, V. Meyer, C. J. Myatt, M. Rowe, Q. A. Turchette, W. M. Itano, D. J. Wineland, and C. Monroe, Experimental entanglement of four particles, *Nature* **404**, 256 (2000).
- [2] V. Meyer, M. A. Rowe, D. Kielpinski, C. A. Sackett, W. M. Itano, C. Monroe, and D. J. Wineland, Experimental demonstration of entanglement-enhanced rotation angle estimation using trapped ions, *Phys. Rev. Lett.* **86**, 5870 (2001).

- [3] D. Leibfried, B. DeMarco, V. Meyer, D. Lucas, M. Barrett, J. Britton, W. M. Itano, B. Jelenković, C. Langer, T. Rosenband, and D. J. Wineland, Experimental demonstration of a robust, high-fidelity geometric two ion-qubit phase gate, *Nature* **422**, 412 (2003).
- [4] D. Leibfried, M. D. Barrett, T. Schaetz, J. Britton, J. Chiaverini, W. M. Itano, J. D. Jost, C. Langer, and D. J. Wineland, Toward Heisenberg-limited spectroscopy with multiparticle entangled states, *Science* **304**, 1476 (2004).
- [5] D. Leibfried, E. Knill, S. Seidelin, J. Britton, R. B. Blakestad, J. Chiaverini, D. B. Hume, W. M. Itano, J. D. Jost, C. Langer, R. Ozeri, R. Reichle, and D. J. Wineland, Creation of a six-atom ‘Schrödinger cat’ state, *Nature* **438**, 639 (2005).
- [6] J. Estève, C. Gross, A. Weller, S. Giovanazzi, and M. K. Oberthaler, Squeezing and entanglement in a Bose–Einstein condensate, *Nature* **455**, 1216 (2008).
- [7] J. Appel, P. J. Windpassinger, D. Oblak, U. B. Hoff, N. Kjærgaard, and E. S. Polzik, Mesoscopic atomic entanglement for precision measurements beyond the standard quantum limit, *PNAS* **106**, 10960 (2009).
- [8] I. D. Leroux, M. H. Schleier-Smith, and V. Vuletić, Implementation of cavity squeezing of a collective atomic spin, *Phys. Rev. Lett.* **104**, 073602 (2010).
- [9] M. H. Schleier-Smith, I. D. Leroux, and V. Vuletić, States of an ensemble of two-level atoms with reduced quantum uncertainty, *Phys. Rev. Lett.* **104**, 073604 (2010).
- [10] C. Gross, T. Zibold, E. Nicklas, J. Estève, and M. K. Oberthaler, Nonlinear atom interferometer surpasses classical precision limit, *Nature* **464**, 1165 (2010).
- [11] M. F. Riedel, P. Böhi, Y. Li, T. W. Hänsch, A. Sinatra, and P. Treutlein, Atom-chip-based generation of entanglement for quantum metrology, *Nature* **464**, 1170 (2010).
- [12] I. D. Leroux, M. H. Schleier-Smith, and V. Vuletić, Orientation-dependent entanglement lifetime in a squeezed atomic clock, *Phys. Rev. Lett.* **104**, 250801 (2010).
- [13] A. Louchet-Chauvet, J. Appel, J. J. Renema, D. Oblak, N. Kjaergaard, and E. S. Polzik, Entanglement-assisted atomic clock beyond the projection noise limit, *New J. Phys.* **12**, 065032 (2010).
- [14] Z. L. Chen, J. G. Bohnet, S. R. Sankar, J. Y. Dai, and J. K. Thompson, Conditional spin squeezing of a large ensemble via the vacuum rabi splitting, *Phys. Rev. Lett.* **106**, 133601 (2011).
- [15] T. Monz, P. Schindler, J. T. Barreiro, M. Chwalla, D. Nigg, W. A. Coish, M. Harlander, W. Hänsel, M. Hennrich, and R. Blatt, 14-qubit entanglement: Creation and coherence, *Phys. Rev. Lett.* **106**, 130506 (2011).
- [16] B. Lücke, M. Scherer, J. Kruse, L. Pezzé, F. Deuretzbacher, P. Hyllus, O. Topic, J. Peise, W. Ertmer, J. Arlt, L. Santos, A. Smerzi, and C. Klempt, Twin matter waves for interferometry beyond the classical limit, *Science* **334**, 773 (2011).
- [17] C. D. Hamley, C. S. Gerving, T. M. Hoang, E. M. Bookjans, and M. S. Chapman, Spin-nematic squeezed vacuum in a quantum gas, *Nat. Phys.* **8**, 305 (2012).
- [18] R. J. Sewell, M. Koschorreck, M. Napolitano, B. Dubost, N. Behbood, and M. W. Mitchell, Magnetic sensitivity beyond the projection noise limit by spin squeezing, *Phys. Rev. Lett.* **109**, 253605 (2012).
- [19] T. Berrada, S. van Frank, R. Bücker, T. Schumm, J.-F. Schaff, and J. Schmiedmayer, Integrated Mach-Zehnder interferometer for Bose-Einstein condensates, *Nat. Commun.* **4**, 2077 (2013).
- [20] C. F. Ockeloen, R. Schmied, M. F. Riedel, and P. Treutlein, Quantum metrology with a scanning probe atom interferometer, *Phys. Rev. Lett.* **111**, 143001 (2013).
- [21] R. J. Sewell, M. Napolitano, N. Behbood, G. Colangelo, F. Martin Ciurana, and M. W. Mitchell, Ultrasensitive atomic spin measurements with a nonlinear interferometer, *Phys. Rev. X* **4**, 021045 (2014).
- [22] H. Strobel, W. Muessel, D. Linnemann, T. Zibold, D. B. Hume, L. Pezzè, A. Smerzi, and M. K. Oberthaler, Fisher information and entanglement of non-Gaussian spin states, *Science* **345**, 424 (2014).
- [23] J. G. Bohnet, K. C. Cox, M. A. Norcia, J. M. Weiner, Z. Chen, and J. K. Thompson, Reduced spin measurement back-action for a phase sensitivity ten times beyond the standard quantum limit, *Nat. Photon.* **8**, 731 (2014).
- [24] W. Muessel, H. Strobel, D. Linnemann, D. B. Hume, and M. K. Oberthaler, Scalable spin squeezing for quantum-enhanced magnetometry with Bose-Einstein condensates, *Phys. Rev. Lett.* **113**, 103004 (2014).
- [25] W. Muessel, H. Strobel, D. Linnemann, T. Zibold, B. Juliá-Díaz, and M. K. Oberthaler, Twist-and-turn spin squeezing in Bose-Einstein condensates, *Phys. Rev. A* **92**, 023603 (2015).
- [26] G. Barontini, L. Hohmann, F. Haas, J. Estève, and J. Reichel, Deterministic generation of multiparticle entanglement by quantum Zeno dynamics, *Science* **349**, 1317 (2015).
- [27] O. Hosten, N. J. Engelsen, R. Krishnakumar, and M. A. Kasevich, Measurement noise 100 times lower than the quantum-projection limit using entangled atoms, *Nature* **529**, 505 (2016).
- [28] K. C. Cox, G. P. Greve, J. M. Weiner, and J. K. Thompson, Deterministic squeezed states with collective measurements and feedback, *Phys. Rev. Lett.* **116**, 093602 (2016).
- [29] J. G. Bohnet, B. C. Sawyer, J. W. Britton, M. L. Wall, A. M. Rey, M. Foss-Feig, and J. J. Bollinger, Quantum spin dynamics and entanglement generation with hundreds of trapped ions, *Science* **352**, 1297 (2016).
- [30] I. Kruse, K. Lange, J. Peise, B. Lücke, L. Pezzè, J. Arlt, W. Ertmer, C. Lisdat, L. Santos, A. Smerzi, and C. Klempt, Improvement of an atomic clock using squeezed vacuum, *Phys. Rev. Lett.* **117**, 143004 (2016).
- [31] Y.-Q. Zou, L.-N. Wu, Q. Liu, X.-Y. Luo, S.-F. Guo, J.-H. Cao, M. K. Tey, and L. You, Beating the classical precision limit with spin-1 Dicke states of more than 10,000 atoms, *PNAS* **115**, 6381 (2018).
- [32] A. Omran, H. Levine, A. Keesling, G. Semeghini, T. T. Wang, S. Ebadi, H. Bernien, A. S. Zibrov, H. Pichler, S. Choi, J. Cui, M. Rossignolo, P. Rembold, S. Montangero, T. Calarco, M. Endres, M. Greiner, V. Vuletić, and M. D. Lukin, Generation and manipulation of Schrödinger cat states in Rydberg atom arrays, *Science* **365**, 570 (2019).
- [33] C. Song, K. Xu, H. K. Li, Y.-R. Zhang, X. Zhang, W. X. Liu, Q. J. Guo, Z. Wang, W. H. Ren, J. Hao, H. Feng, H. Fan, D. N. Zheng, D.-W. Wang, H. Wang, and S.-Y. Zhu, Generation of multicomponent atomic Schrödinger cat states of up to 20 qubits, *Science* **365**, 574 (2019).

- [34] R. Krischek, C. Schwemmer, W. Wieczorek, H. Weinfurter, P. Hyllus, L. Pezzé, and A. Smerzi, Useful multiparticle entanglement and sub-shot-noise sensitivity in experimental phase estimation, *Phys. Rev. Lett.* **107**, 080504 (2011).
- [35] L.-Z. Liu, Y.-Z. Zhang, Z.-D. Li, R. Zhang, X.-F. Yin, Y.-Y. Fei, L. Li, N.-L. Liu, F. Xu, Y.-A. Chen, and J.-W. Pan, Distributed quantum phase estimation with entangled photons, *Nat. Photon.* **15**, 137 (2021).
- [36] L. Pezzè, A. Smerzi, M. K. Oberthaler, R. Schmied, and P. Treutlein, Quantum metrology with nonclassical states of atomic ensembles, *Rev. Mod. Phys.* **90**, 035005 (2018).
- [37] C. Song, K. Xu, W. X. Liu, C. P. Yang, S. B. Zheng, H. Deng, Q. W. Xie, K. Q. Huang, Q. J. Guo, L. B. Zhang, P. F. Zhang, D. Xu, D. N. Zheng, X. B. Zhu, H. Wang, Y. A. Chen, C. Y. Lu, S. Y. Han, and J. W. Pan, 10-qubit entanglement and parallel logic operations with a superconducting circuit, *Phys. Rev. Lett.* **119**, 180511 (2017).
- [38] M. Gessner, A. Smerzi, and L. Pezzè, Metrological nonlinear squeezing parameter, *Phys. Rev. Lett.* **122**, 090503 (2019).
- [39] W. Zhong, Z. Sun, J. Ma, X. Wang, and F. Nori, Fisher information under decoherence in Bloch representation, *Phys. Rev. A* **87**, 022337 (2013).
- [40] S. L. Braunstein and C. M. Caves, Statistical distance and the geometry of quantum states, *Phys. Rev. Lett.* **72**, 3439 (1994).